Constructing Slow Invariant Manifolds for Closed Reactive Systems

Ashraf N. Al-Khateeb,[a] Joseph M. Powers,[a] Samuel Paolucci,[a] Andrew J. Sommese,[b] Jeffrey A. Diller,[b] Jonathan D. Hauenstein,[b] and Joshua D. Mengers[a]

University of Notre Dame, Notre Dame, Indiana, 46556-5637, USA

(Received March 6, 2009)

Abstract

Reactive systems' slow dynamic behavior is approximated well by evolution on manifolds of dimension lower than that of the full composition spaces. This work addresses the construction of one-dimensional slow invariant manifolds for dynamical systems arising from modeling unsteady spatially homogeneous closed reactive systems. The relation between the systems' slow dynamics, described by the constructed manifolds, and thermodynamics is clarified. It is shown that other than identifying the equilibrium state, traditional equilibrium thermodynamic potentials provide no guidance in the systems' actual slow invariant manifolds. The construction technique is based on analyzing the composition space of the reactive system. The system's finite and infinite equilibria are calculated using a homotopy continuation method. The slow invariant manifolds are constructed by calculating heteroclinic orbits which connect appropriate equilibria to the unique stable physical equilibrium point. Application of the method to several realistic reactive systems, including a detailed hydrogen-air kinetics model, reveals that constructing the actual slow invariant manifolds can be computationally efficient and algorithmically easy.

Keywords: Manifold, Dimensional reduction, Thermodynamics, Detailed kinetics.

[a]Department of Aerospace and Mechanical Engineering.

[b]Department of Mathematics.

I. INTRODUCTION

Modeling physical problems of multi-scale nature is a formidable task, even with modern computational capabilities. Typical examples are found in atmospheric chemistry,[1] biochemistry,[2] and combustion,[3] where a number of physical and chemical processes that occur at different scales exist. For simulation purposes, the presence of a broad range of scales incurs a large computational cost.[4] In the case of combustion, this cost increases with the number of species and the number of reactions.[5] Also, as the scales' range widens, solution verification becomes increasingly difficult. In the literature, numerous methods based on several approaches have been proposed to efficiently simplify and reduce the computational cost of simulating reactive systems described by detailed kinetics.[6–23] The main challenge for these methods is to simplify the model equations without significant loss of accuracy.

For spatially homogeneous reactive systems, reaction dynamics are described by a set of non-linear coupled ordinary differential equations (ODEs). The solutions of this set of ODEs are represented by trajectories in the species composition space. Each trajectory represents the reactive system's evolution with time for a specific initial condition. After a short transient, the evolved trajectories seem to quickly be attracted to a special trajectory and stay exponentially close to it until they reach equilibrium in infinite time.[12] The reactive system's slow modes are the only active ones on this special trajectory. This implies that the system's slow dynamics can be described by these attractors or manifolds which are of smaller dimension than the full composition space dimension.[17] Thus, identifying this manifold for a reactive system makes it possible to reduce the computational cost by filtering the system's fast modes. Such an approach relies on identifying these manifolds within the species composition space which describe the slow dynamics of a reactive system.[19–23]

The dimension reduction approach can significantly reduce the computational cost of modeling a detailed kinetics reactive system.[21] This approach is based on representing the chemistry of a reactive system's variables in terms of the chemistry of a reduced number of variables. Within the dimension reduction approach, two major techniques exist. The first set of methods employ local linear time scale analysis to separate the system's modes into fast and slow, such as intrinsic low-dimensional manifolds (ILDM),[10] computational singular perturbation (CSP),[12–14] and global quasi-linearization (GQL).[11] The dynamics are segregated using chemical bases. These bases are generated *a priori* in the ILDM and GQL,

while in the CSP they are estimated locally by iteration. Although ILDM is more efficient than CSP, it is less accurate.[24] Furthermore, the calculated manifolds using ILDM and GQL are not invariant.[25]

The second set of methods, which is the main subject of this work, employs a geometrical approach to describe the multi-scale kinetics. Examples include the quasi-steady state assumption (QSSA),[26] iterative methods,[15–17] the minimal entropy production trajectory (MEPT) method,[19,27] the method of invariant manifold (MIM),[20] the rate-controlled constrained equilibrium (RCCE) method,[28,29] and the invariant constrained equilibrium edge preimage curve method (ICE-PIC).[21,30] The iterative methods are the most accurate among these approaches.[31,32] These methods are based on constructing the attractive invariant manifold from the system trajectories. Although these methods have a rapid rate of convergence, they require a sufficiently accurate guess to converge.[17] On the other hand, MEPT, MIM, RCCE and ICE-PIC employ classical thermodynamics to construct the attractive manifolds. The MEPT approach relies on the concept of minimum entropy production.[33] Utilizing such a principle allows classical thermodynamics quantities to be used away from equilibrium, though the validity of this principle has been called into question in other fields, *e.g.* heat diffusion.[34] The RCCE, MIM and ICE-PIC approaches rely on employing equilibrium thermodynamics potentials away from the equilibrium state. By minimizing the appropriate classical thermodynamics quantities, at some point in the procedure, their low-dimensional manifolds are constructed. Furthermore, the ICE-PIC method is computationally expensive,[21] and it is not more accurate than ILDM, though the constructed manifold is invariant.

The slow invariant manifold (SIM) for a reactive system is a subspace in the species composition space. It describes the asymptotic structure of the invariant attracting reactive system's trajectories during their relaxation toward equilibrium. All previously discussed methods, and any other method based on them, are approximating the reactive systems' actual SIMs. The only exception is the technique presented by Davis and Skodje.[17] It is based on a global phase space analysis of the full dynamics of a reactive system. Such construction has been done for small model systems.[17,22] The present paper offers the first construction of a SIM for a realistic detailed kinetics system.

The main goal of this work is to identify a reactive system's actual one dimensional (1-D) SIM. We confine our attention to isothermal systems, although extension to non-

isothermal systems is straightforward. This paper is organized as follows. In Sec. II the mathematical foundation is presented for closed isothermal spatially homogenous reactive systems. Then, in Sec. III the proposed method to construct the actual 1-D SIM is presented in a geometric frame. In Sec. IV, several test cases are introduced, and their actual 1-D SIMs are constructed. Moreover, comparison to other methods is conducted. Then, results for a detailed kinetics hydrogen-air reactive system are presented, and lastly conclusions are stated.

II. MATHEMATICAL BACKGROUND

In this section, a brief description of the governing equations is presented. The superscript $(^o)$ denotes evaluation at reference pressure; quantities with superscripts $(^*)$ and $(^e)$ correspond, respectively, to the initial state and to the equilibrium state, and quantities with an overbar $(\bar{})$ denote the evaluation of these quantities on a molar-basis, *i.e.* per unit mole.

A. Model equations

We consider a closed, spatially homogenous, premixed reactive mixture of calorically imperfect ideal gases described by detailed mass-action kinetics. The mixture is confined in a volume V at temperature T and pressure p. This mixture consists of N species composed of L atomic elements which undergo J reversible reactions of the form

$$\sum_{i=1}^{N} \nu'_{ij} \chi_i = \sum_{i=1}^{N} \nu''_{ij} \chi_i, \quad j = 1, \ldots, J. \tag{1}$$

Here, χ_i is the chemical symbol of species i, and for the j^{th} reaction, ν'_{ij} and ν''_{ij} are the stoichiometric coefficients of species i, denoting the number of moles of reactants and products, respectively. For such mixtures, the total mass (M) remains constant throughout the reaction process, and for each reaction in the mechanism the mass of each element is conserved. Total mass and element mass balances are enforced by the following linear relations,

$$\mathsf{M} = \sum_{i=1}^{N} \bar{M}_i n_i = \sum_{i=1}^{N} \bar{M}_i n_i^*, \tag{2a}$$

$$\sum_{i=1}^{N} \phi_{li} \nu_{ij} = 0, \quad l = 1, \ldots, L, \quad j = 1, \ldots, J, \tag{2b}$$

where $\bar{M}_i, n_i$ and ϕ_{li} are, respectively, the molecular mass of species i, the number of moles of species i, and the element index matrix, which provides the number of moles of element l in species i. Also, $\nu_{ij} = \nu''_{ij} - \nu'_{ij}$ is the stoichiometric matrix, which gives the net stoichiometric coefficient for species i in reaction j. Equation (2b) demands that ν_{ij} lie in the right null space of ϕ_{li}. In general, ϕ_{li} and ν_{ij} are non-square matrices of dimensions $L \times N$ and $N \times J$, respectively. However, ϕ_{li} is of full rank, while ν_{ij} is of rank $R \leq (N - L)$; commonly $R = (N - L)$. In this work, we focus on systems in which $J \geq R$. However, for the less common systems in which $J < R$, the presented analysis can be easily modified.

The change in the number of moles of species i with time (t) due to chemical reaction is described by the following system:[35]

$$\frac{dn_i}{dt} = V \sum_{j=1}^{J} \nu_{ij} r_j, \qquad i = 1, \ldots, N, \tag{3a}$$

$$n_i|_{t=0} = n_i^*, \qquad i = 1, \ldots, N, \tag{3b}$$

where

$$r_j = k_j \left(\prod_{i=1}^{N} \left(\frac{n_i}{V} \right)^{\nu'_{ij}} - \frac{1}{K_j^c} \prod_{i=1}^{N} \left(\frac{n_i}{V} \right)^{\nu''_{ij}} \right), \quad j = 1, \ldots, J, \tag{4}$$

is the reaction rate given by the law of mass action. Here, for the j^{th} reaction, k_j and K_j^c are, respectively, the temperature-dependent Arrhenius kinetic rates given by

$$k_j = A_j \, T^{\beta_j} \, \exp\left(\frac{-\bar{E}_j}{\bar{\Re} T} \right), \quad j = 1, \ldots, J, \tag{5}$$

and the equilibrium "constants" given by

$$K_j^c = \left(\frac{p^o}{\bar{\Re} T} \right)^{\sum_{i=1}^{N} \nu_{ij}} \exp\left(- \frac{\sum_{i=1}^{N} \bar{\mu}_i^o \nu_{ij}}{\bar{\Re} T} \right), \quad j = 1, \ldots, J. \tag{6}$$

In Eqs. (5) and (6), $\bar{\Re} = 8.314 \times 10^7 \; erg/mol/K$ is the universal gas constant, and for each reaction the quantities A_j, β_j, and $\bar{E}_j$ represent the collision frequency factor, the temperature-dependency exponent, and the activation energy, respectively. Also, $\bar{\mu}_i^o$ are the chemical potentials given by

$$\bar{\mu}_i^o = \bar{M}_i \left(h_i - T s_i^o \right), \quad i = 1, \ldots, N. \tag{7}$$

Here, h_i and s_i^o are the specific enthalpy and the specific entropy of species i. For ideal gases, h_i and s_i^o are constant for a given T.

B. Thermodynamic conditions

Considering a mixture of calorically imperfect ideal gases implies that the thermal state equation is

$$p = \frac{\bar{\Re} T}{V} \sum_{i=1}^{N} n_i. \tag{8}$$

Also, the mixture Gibbs free energy (G) is given by the following relation,[36]

$$G = \sum_{i=1}^{N} n_i \bar{\mu}_i, \tag{9a}$$

where,

$$\bar{\mu}_i = \bar{\mu}_i^o + \bar{\Re} T \ln \left(\frac{p \; n_i}{p^o \sum_{j=1}^{N} n_j} \right), \quad i = 1, \ldots, N. \tag{9b}$$

This thermodynamic property is of special interest. The global minimum of G corresponds to the reactive system's equilibrium state,[37] which is identified by the following relation

$$\sum_{i=1}^{N} \nu_{ij} \bar{\mu}_i = 0, \quad j = 1, \ldots, J. \tag{10}$$

Another thermodynamic property of special interest in this work is the mixture entropy (S), which is defined as

$$S = \sum_{i=1}^{N} n_i \bar{s}_i. \tag{11a}$$

where,

$$\bar{s}_i = \bar{M}_i s_i^o - \bar{\Re} \ln \left(\frac{p \; n_i}{p^o \sum_{j=1}^{N} n_j} \right). \tag{11b}$$

The differential change of S is postulated by the second law of thermodynamics,[37] though it stated differently in non-equilibrium thermodynamics than classical thermodynamics.[36] In non-equilibrium thermodynamics, the differential change of S is denoted as[38]

$$dS = d_e S + d_i S, \tag{12a}$$

in which $d_e S$ is the change in entropy due to the system's exchange of matter and energy with its surroundings, and

$$d_i S = -\frac{1}{T} \sum_{i=1}^{N} \bar{\mu}_i dn_i, \tag{12b}$$

is the change in entropy due to irreversible processes within the system. Thus, an expression for the irreversibility production rate (σ), also known as the entropy production rate, is introduced as[33]

$$\sigma = \frac{d_i S}{dt} = -\frac{1}{T}\sum_{i=1}^{N} \bar{\mu}_i \frac{dn_i}{dt}. \tag{13}$$

Similar to G, σ is a convex function in composition space with a global minimum at the reactive system's equilibrium point.

C. Governing equations

The complete system, Eq. (3), defines an N-dimensional composition space. But, in any closed reactive system the total number of moles of each element is conserved. By multiplying both sides of Eq. (3a) by ϕ_{li}, summing the result from $i = 1$ to N, employing Eq. (2b) to set the right side to zero, integrating the resulting homogeneous differential equation, and applying the initial condition, Eq. (3b), we obtain

$$\sum_{i=1}^{N} \phi_{li} n_i = \sum_{i=1}^{N} \phi_{li} n_i^*, \quad l = 1, \ldots, L. \tag{14}$$

Generally, Eq. (14) is an underconstrained linear system of L equations for the N values of n_i[39]. This implies it has solutions of the following form

$$n_i = n_i^* + \mathsf{M}\left(\sum_{k=1}^{R} \mathcal{D}_{ik} z_k\right), \quad i = 1, \ldots, N. \tag{15}$$

Here, $z_k = n_k/\mathsf{M}, k = 1, \ldots, R$, is a reduced composition variable which physically represents the number of moles of species k in M, and $\mathcal{D}_{ik}$ is a dimensionless constant matrix of size $N \times R$ and has a full rank R. Each column vector of $\mathcal{D}_{ik}$ is linearly independent of the remaining column vectors. However, $\mathcal{D}_{ik}$ is not unique; it can be constructed in several ways. In this work, $\mathcal{D}_{ik}$ is constructed using the following procedure. First, a row-echelon form of the ν_{ij} matrix is obtained by performing a series of row operations on Eq. (3a). The number of non-zero rows in the row-echelon form of ν_{ij} is the rank of ν_{ij} and $\mathcal{D}_{ik}$, since ν_{ij} and $\mathcal{D}_{ik}$ span the same column space. We use elementary row operations to identify the $N \times N$ lower triangular matrix ($\mathbf{L}$) which, when matrix multiplied with Eq. (3a) $\mathbf{L} \cdot d\mathbf{n}/dt = V\mathbf{U} \cdot \mathbf{r}$, where $\mathbf{U} = \mathbf{L} \cdot \boldsymbol{\nu}$ is an upper triangular matrix of dimension $N \times R$. This non-unique matrix describes the system's linear constraints, which are obtained by integrating the $N - R$

homogenous ODEs that are obtained as a result of reduction to the row-echelon form. Then, the $\mathcal{D}_{ik}$ matrix is constructed such that the first R row vectors of it are set in the reduced row-echelon form, while the other row vectors are obtained using $\mathbf{L}$ to reflect the system constraints. A detailed example will be given later to illustrate the construction of $\mathcal{D}_{ik}$ for a realistic reactive system.

Equation (15) allows the N species to be represented in terms of R dependent variables. First, take the time derivative of Eq. (15) to get

$$\frac{dn_i}{dt} = \mathsf{M}\left(\sum_{k=1}^{R} \mathcal{D}_{ik}\frac{dz_k}{dt}\right), \quad i = 1, \ldots, N. \tag{16a}$$

Now, by substituting Eq. (3a) into Eq. (16a), we obtain

$$\frac{V}{\mathsf{M}}\dot{\omega}_i = \left(\sum_{k=1}^{R} \mathcal{D}_{ik}\frac{dz_k}{dt}\right), \quad i = 1, \ldots, N, \tag{16b}$$

where

$$\dot{\omega}_i = \sum_{j=1}^{J} \nu_{ij} r_j, \quad i = 1, \ldots, N, \tag{16c}$$

is the molar production rate per unit volume of species i. In Gibbs notation, Eq. (16b) is written as

$$\frac{V}{\mathsf{M}}\dot{\boldsymbol{\omega}} = \mathcal{D} \cdot \frac{d\mathbf{z}}{dt}, \quad \mathbf{z} \in \mathbb{R}^R, \quad \dot{\boldsymbol{\omega}} \in \mathbb{R}^N. \tag{16d}$$

Since $\mathcal{D}$ is non-square, we take the matrix product of both sides of Eq. (16d) with $\mathcal{D}^T$ to obtain

$$\frac{V}{\mathsf{M}}\mathcal{D}^T \cdot \dot{\boldsymbol{\omega}} = \mathcal{D}^T \cdot \mathcal{D} \cdot \frac{d\mathbf{z}}{dt}, \quad \mathbf{z} \in \mathbb{R}^R, \quad \dot{\boldsymbol{\omega}} \in \mathbb{R}^N. \tag{16e}$$

Then, to eliminate $\mathcal{D}$ from the right hand side of Eq. (16e), we take the matrix product of both sides by $\left(\mathcal{D}^T \cdot \mathcal{D}\right)^{-1}$. Consequently, the rate of evolution of the species in the reactive mixture is governed by

$$\frac{dz_k}{dt} = \dot{w}_k, \qquad k = 1, \ldots, R, \tag{17a}$$

$$z_k|_{t=0} = z_k^*, \qquad k = 1, \ldots, R, \tag{17b}$$

where

$$\dot{w}_k = \frac{1}{\rho}\sum_{j=1}^{R}\left[\left(\sum_{i=1}^{N} \mathcal{D}_{ik}\mathcal{D}_{ij}\right)^{-1}\left(\sum_{i=1}^{N} \mathcal{D}_{ij}\ \dot{\omega}_i\right)\right], \quad k = 1, \ldots, R, \tag{18}$$

is the molar production rate of species k in the reduced composition space, and $\rho = \mathsf{M}/V$ is the mixture mass density. So, the reactive system's solutions, represented as trajectories, move within the reduced composition space $\mathbb{R}^R$ where $\mathbb{R}^R \subset \mathbb{R}^N$.

III. METHODOLOGY

From a geometric point of view, the species specific moles $\mathbf{z}$ correspond to a vector in the Euclidian composition space $\mathbb{R}^R$. This vector is given by the following relation

$$\mathbf{z} = \mathcal{L}(\mathbf{n}) \quad \big| \; \mathcal{L} : \left(\mathbb{R}^N \to \mathbb{R}^R\right) , \tag{19}$$

where

$$\mathcal{L}(\mathbf{n}) = \frac{1}{\mathsf{M}} \left(\mathcal{D}^T \cdot \mathcal{D}\right)^{-1} \cdot \mathcal{D}^T \cdot (\mathbf{n} - \mathbf{n}^*) , \tag{20}$$

is a linear operator that accounts for all the system's constrains. The evolution of $\mathbf{z}$ in time is described as an autonomous dynamical system of the standard form

$$\frac{d\mathbf{z}}{dt} = \mathbf{f}(\mathbf{z}) , \quad \mathbf{z} \in \mathbb{R}^R, \tag{21}$$

where $\mathbf{f}$ is a set of R non-linear coupled algebraic functions. For our isothermal system, these functions are polynomials of degree `d` connected with a given reaction mechanism.

The construction method of the SIM is based on identifying all the equilibria of the dynamical system that describes the species evolution, Eq. (21). In general, the set of equilibria of such functions is complex;

$$\mathbf{z}^e \in \mathbb{C}^R \, | \mathbf{f}(\mathbf{z}^e) = \mathbf{0} . \tag{22}$$

Also, as demonstrated by Perko,[40] the set of equilibria $\mathbf{z}^e$ contains finite and infinite equilibria, and both classes will be of interest. Furthermore, the equilibria can be positive dimensional continua.[41] Here, `Bertini`,[42] a code based on homotopy continuation, is used to obtain the system's equilibria to any desired accuracy. Then, the equilibria are connected via trajectories obtained by numerical integration of the species evolution equations using any computationally inexpensive scheme; here we use the fourth-order Runge-Kutta scheme. Finally, we are able to identify the 1-D SIM which describes the asymptotic structure of the invariant attracting trajectories.

In this work, the kinetic rates and the thermodynamic properties are calculated using the public domain edition of the `CHEMKIN` package.[43,44] The computational time to construct a 1-D SIM is less than five minute on a MacBookPro 2.16 GHz machine. All calculations have been performed to 100 significant digits. However, all the listed results have been rounded to three significant digits. Integer values indicate that the reported numbers are exact.

A. Equilibria; `Bertini`

Bertini is a software package designed to compute the solutions of polynomial systems over $\mathbb{C}$ using homotopy continuation. Polynomial systems that arise from chemical reactions are often poorly scaled which can lead to numerical difficulties when computing the solutions. When Bertini is used to solve polynomial systems as discussed in this work, the polynomial systems are first rescaled using SCLGEN.[45] SCLGEN is an algorithm that uses both a change of variables and equation scaling to rescale the given polynomial system into one which has coefficients of reduced variability and centered about unity. For example, if $f_1(z_1,\ldots,z_R),\ldots,f_R(z_1,\ldots,z_R)$ are polynomials, SCLGEN computes real constants $\alpha_1,\ldots,\alpha_R$ and $\beta_1,\ldots,\beta_R$ to define the rescaled system $g_1(x_1,\ldots,x_R),\ldots,g_R(x_1,\ldots,x_R)$ by

$$\mathbf{g}(\mathbf{x}) = \boldsymbol{\beta}\cdot\mathbf{f}(\boldsymbol{\alpha}\cdot\mathbf{z}), \quad \{\mathbf{g},\mathbf{f},\mathbf{z},\boldsymbol{\alpha},\boldsymbol{\beta}\}\in\mathbb{R}^R.$$

Reference 41 provides a detailed description of using homotopy continuation to describe all solutions to a given polynomial system.

B. Finite equilibria

To obtain the dynamical system's finite equilibria, we find all the $\mathbf{z}^e$ that satisfy $\mathbf{f}(\mathbf{z}^e)=\mathbf{0}$. One of these finite equilibria is the reactive system's physical equilibrium point. This critical point is of special interest; it represents the global minimum of G. Moreover, it is the only critical point located inside the physically accessible domain ($\mathbb{S}$),[39] which is defined as a subspace within the reduced composition space where all the species are positive semi-definite and finite;

$$\mathbb{S}\subset\mathbb{R}^R \mid \mathbf{n}\geq\mathbf{0}. \tag{23}$$

The rest of the finite equilibria are located outside $\mathbb{S}$; they are non-physical since at least one of the species mole numbers is negative, $n_i<0$.

Next, the dynamic behavior of the system within the neighborhood of each finite equilibrium is investigated by employing standard linearization techniques. For a hyperbolic equilibrium,[40] the Hartman-Grobman theorem is used to reveal its dynamical character. For a non-hyporbolic equilibrium, the Hartman-Grobman theorem is not applicable, so the normal form theory[40] is utilized to reveal the dynamical character of the equilibrium. First, we linearize the system in the neighborhood of each equilibrium. We start by defining the perturbation from the equilibrium as $\mathbf{z}' = \mathbf{z} - \mathbf{z}^e$. The dynamics can be described locally as

$$\frac{d\mathbf{z}'}{dt} = \mathbf{J}^e \cdot \mathbf{z}' + \mathcal{O}\left(\mathbf{z}'^2\right). \tag{24}$$

Here,

$$\mathbf{J}^e = \left.\frac{\partial \mathbf{f}}{\partial \mathbf{z}}\right|_{\mathbf{z}=\mathbf{z}^e} \tag{25}$$

is the constant Jacobian matrix evaluated at an equilibrium. The stability of each equilibrium is determined by examining the eigenvalue spectrum λ_i of $\mathbf{J}^e$ and the corresponding eigenvectors υ_i. The local time scales over which the dynamical system, Eq. (21), evolves are given by the reciprocal of the real part of the system's eigenvalues, $1/|Re(\lambda_i)|$.

In general, the eigenvalues are complex, where the reciprocal of the real parts provides the scales of the amplitude growth, and the reciprocal of the imaginary parts represents the period of oscillations. The physical equilibrium point must be a stable node;[46] in other words, all the eigenvalues of $\mathbf{J}^e$ are real and negative. Furthermore, the ratio between the largest and smallest time scales identifies the system's stiffness. In addition, the eigenvector associated with the least negative eigenvalue represents the system's slowest mode or direction in phase space along which the trajectories approach the equilibrium. Similarly, the eigenvector associated with the largest eigenvalue represents the system's fastest mode.

C. Infinite equilibria

To identify the dynamical system's infinite equilibria, the projective space technique is employed.[41,47] This technique maps the critical points at infinity into the finite domain where they can be easily computed. The projective space mapping consists of the following

one-to-one transformation:

$$Z_k = \frac{1}{z_k}, \qquad k \in \{1, \ldots, R\}, \tag{26a}$$

$$Z_i = \frac{z_i}{z_k}, \qquad i \neq k, \quad i = 1, \ldots, R, \tag{26b}$$

where z_k is any arbitrarily selected dependent variable, and $\mathbf{Z}$ are the state variables in the projective space.

The projective space technique has the disadvantage of introducing a singularity in the dynamical system. To overcome this difficulty, we define a transformed independent variable τ in the projective space which is related to t in the original space as follows:

$$\frac{dt}{d\tau} = (Z_k)^{\mathtt{d}-1}, \tag{27}$$

where we recall that $\mathtt{d}$ is the maximum degree of polynomials in $\mathbf{f}$. By employing this mapping, the original dynamical system, Eq. (21), is recast in the projective space in the following form:

$$\frac{d\mathbf{Z}}{d\tau} = \frac{d}{d\tau}\begin{pmatrix} Z_0 \\ Z_1 \\ \vdots \\ Z_{k-1} \\ Z_k \\ Z_{k+1} \\ \vdots \\ Z_R \end{pmatrix} = Z_k^{\mathtt{d}} \cdot \begin{pmatrix} Z_k^{-1} \\ f_1(Z_1, \ldots, Z_R) - Z_1 f_k(Z_1, \ldots, Z_R) \\ \vdots \\ f_{k-1}(Z_1, \ldots, Z_R) - Z_{k-1} f_k(Z_1, \ldots, Z_R) \\ -Z_k f_k(Z_1, \ldots, Z_R) \\ f_{k+1}(Z_1, \ldots, Z_R) - Z_{k+1} f_k(Z_1, \ldots, Z_R) \\ \vdots \\ f_R(Z_1, \ldots, Z_R) - Z_R f_k(Z_1, \ldots, Z_R) \end{pmatrix} = \mathbf{F}(\mathbf{Z}), \tag{28}$$

where we denoted $Z_0 = t$. The finite equilibria satisfying $\mathbf{F}(\mathbf{Z}^e) = \mathbf{0}$ of the resulting dynamical system, Eq. (28), represent the infinite equilibria of the original dynamical system, Eq. (21). We note here that $\mathbf{Z} \in \mathbb{R}^{R+1}$, though the value of Z_0^e is irrelevant.

D. Construction method

Here, the procedure for constructing the closed spatially homogenous reactive system's 1-D SIM is presented. In this, the following conjecture has been found to be useful. At this stage we have no formal proof for it.

Conjecture: *Only the system's isolated real finite and infinite equilibria are relevant to the construction of a 1-D SIM. Furthermore, among these equilibria, only those with one unstable eigenvector direction can be candidate members of the 1-D SIM.*

As a consequence of the first part of the conjecture, the high-dimensional equilibria and the complex equilibria are not relevant to this study. Furthermore, as a consequence of the second part of the conjecture, the real critical points with the following dynamical character are excluded: sinks, sources, saddles with more than one positive eigenvalue, and non-hyperbolic equilibria with more than one positive eigenvalue.

The system's finite and infinite equilibria that satisfy our conjecture will be called candidate equilibria. Starting from each one of these equilibria, a heteroclinic orbit is generated tangent to its unstable direction. This orbit is defined to be a trajectory that connects two critical points. Only heteroclinic orbits that connect to the physical equilibrium are relevant to the construction of the 1-D SIM. In general, the 1-D SIM consists of at most two branches. Among the heteroclinic orbits, two such orbits represent the branches of the system's 1-D SIM. These orbits can be identified since they are the only ones that approach the physical equilibrium point tangent to its slowest mode.

We start the process of SIM construction by generating a heteroclinic orbit from the finite candidate point with the least positive eigenvalue. Then, we check whether the generated orbit approaches the physical equilibrium point in the direction of its slowest mode. Subsequently, if the the physical equilibrium is not located at the origin, another orbit is generated starting from the finite candidate point with the second lowest positive eigenvalue. If both of these orbits approach the physical equilibrium point in the direction of its slowest mode, then these correspond to the SIM's two branches. Otherwise, we generate a new heteroclinic orbit from the finite candidate point with the third lowest eigenvalue, and so on. After using all finite candidate points, we follow the same procedure using the infinite candidate points. This procedure, halts as soon as we construct two heteroclinic orbits that approach the the physical equilibrium point in the direction of its slowest mode. If the system's physical equilibrium is located at the origin of the species composition space, $\mathbf{n}^e = \mathbf{0}$, then the procedure halts after we construct a single branch.

In this work we focus solely on the construction of a 1-D SIM. However, the procedure can be systematically extended to construct higher-dimensional SIMs. This will be reported in a future work.

IV. MODEL PROBLEMS

In this section, we illustrate our strategy for constructing a 1-D SIM using three problems. The first problem is a simple but realistic reactive system. The other two systems have been used in the literature as prototypes for illustrating different techniques of constructing SIMs.

A. Zel'dovich mechanism

One of the common reaction kinetics models is the Zel'dovich mechanism of nitric oxide formation.[26] This mechanism consists of $N = 5$ species, $L = 2$ elements, and $J = 2$ reversible reactions, and the kinetic data is adopted from Baulch *et al.*[48], see Table I. A special case in which the system is isochoric will be considered, and the assigned mixture temperature and volume are $T = 4000\ K$ and $V = 10^3\ cm^3$, respectively. For convenience, the assigned initial number of moles of each species is $\mathbf{n}^* = 10^{-3}\ mol$.

Here, $i = \{1, 2, 3, 4, 5\}$ correspond to the species $\{NO, N, O, O_2, N_2\}$, and $l = \{1, 2\}$ correspond to the elements $\{N, O\}$, respectively. For this system $\boldsymbol{\phi}$ has dimension 2×5:

$$\boldsymbol{\phi} = \begin{pmatrix} 1 & 1 & 0 & 0 & 2 \\ 1 & 0 & 1 & 2 & 0 \end{pmatrix},$$

and $\boldsymbol{\nu}$ has dimension 5×2:

$$\boldsymbol{\nu} = \begin{pmatrix} 1 & -1 \\ -1 & -1 \\ 1 & 1 \\ -1 & 0 \\ 0 & 1 \end{pmatrix}.$$

For the constraint of element conservation for each reaction, Eq. (2b), we have

$$\boldsymbol{\phi} \cdot \boldsymbol{\nu} = \begin{pmatrix} 0 & 0 \\ 0 & 0 \end{pmatrix}.$$

Thus, there are two element constraints in this model.

We start by formulating the set of ODEs that describes this kinetic model. Following

Eq. (3a), we get

$$\frac{d}{dt}\begin{pmatrix} n_1 \\ n_2 \\ n_3 \\ n_4 \\ n_5 \end{pmatrix} = V \begin{pmatrix} 1 & -1 \\ -1 & -1 \\ 1 & 1 \\ -1 & 0 \\ 0 & 1 \end{pmatrix} \begin{pmatrix} r_1 \\ r_2 \end{pmatrix}, \tag{29a}$$

where, from Eq. (4),

$$\begin{aligned} r_1 &= \frac{A_1 T^{\beta_1}}{V^2} \exp\left(\frac{-\bar{E}_1}{\bar{\Re} T}\right)\left(n_2 n_4 - \frac{n_1 n_3}{K_1^c}\right), \\ r_2 &= \frac{A_2 T^{\beta_2}}{V^2} \exp\left(\frac{-\bar{E}_2}{\bar{\Re} T}\right)\left(n_2 n_1 - \frac{n_5 n_3}{K_2^c}\right). \end{aligned}$$

Now, Eq. (29a) defines a real $\mathbb{R}^N$ composition space. To reduce the dimension of this composition space, we construct the matrix $\mathcal{D}_{ik}$. First, we perform a series of row operations on Eq. (29a) to find all of the system constraints; *i.e.* we need to generate the row-echelon form of $\boldsymbol{\nu}$:

$$\begin{pmatrix} 1 & 0 & 0 & 0 & 0 \\ 1 & 1 & 0 & 0 & 0 \\ 0 & 1 & 1 & 0 & 0 \\ \frac{1}{2} & -\frac{1}{2} & 0 & 1 & 0 \\ \frac{1}{2} & \frac{1}{2} & 0 & 0 & 1 \end{pmatrix} \frac{d}{dt}\begin{pmatrix} n_1 \\ n_2 \\ n_3 \\ n_4 \\ n_5 \end{pmatrix} = V \begin{pmatrix} 1 & -1 \\ 0 & -2 \\ 0 & 0 \\ 0 & 0 \\ 0 & 0 \end{pmatrix} \begin{pmatrix} r_1 \\ r_2 \end{pmatrix}, \tag{29b}$$

or in Gibbs notation,

$$\mathbf{L} \cdot \frac{d\mathbf{n}}{dt} = V\left(\mathbf{U} \cdot \mathbf{r}\right).$$

We note that the rank of $\boldsymbol{\nu}$ is $R = 2$ which corresponds to the number of the non-zero rows of $\mathbf{U} = \mathbf{L} \cdot \boldsymbol{\nu}$.

In Eq. (29b) the last three equations are homogenous, so this model contains three linear constraints. Moreover, it implies that the behavior of $\mathbf{n}$ as a function of time is described by the evolution of only two variables: n_1 and n_2. The remaining variables, $\{n_3, n_4, n_5\}$, can be expressed in terms of n_1 and n_2. These expressions are obtained by integrating the three homogenous equations in the system to obtain

$$n_2 + n_3 = c_1, \tag{30a}$$

$$\frac{1}{2}n_1 - \frac{1}{2}n_2 + n_4 = c_2, \tag{30b}$$

$$\frac{1}{2}n_1 + \frac{1}{2}n_2 + n_5 = c_3, \tag{30c}$$

where c_1, c_2 and c_3 are constants that are determined from $\mathbf{n}^*$. Further elementary row operations on Eqs. (30a-30c) reveal the following set:

$$n_1 + n_3 + 2n_4 = \quad c_1 + 2c_2 \quad = n_1^* + n_3^* + 2n_4^*, \tag{31a}$$

$$n_1 + n_2 + 2n_5 = \quad 2c_3 \quad = n_1^* + n_2^* + 2n_5^*, \tag{31b}$$

$$n_1 + n_2 + n_3 + n_4 + n_5 = \; c_1 + c_2 + c_3 \; = \sum_{i=1}^{N} n_i^*. \tag{31c}$$

Equations (31a) and (31b) indicate that the total number of moles of elemental oxygen and nitrogen are conserved. Equation (31c) states that the total number of molecules is constant. This last constraint is a consequence of including only bimolecular reactions in this kinetic model.

Now, by including the dependent variables, Eqs. (30a-30c) can be rearranged to obtain

$$\begin{pmatrix} n_1 \\ n_2 \\ n_3 \\ n_4 \\ n_5 \end{pmatrix} = \begin{pmatrix} 0 \\ 0 \\ c_1 \\ c_2 \\ c_3 \end{pmatrix} + \begin{pmatrix} 1 & 0 \\ 0 & 1 \\ 0 & -1 \\ -\frac{1}{2} & \frac{1}{2} \\ -\frac{1}{2} & -\frac{1}{2} \end{pmatrix} \begin{pmatrix} n_1 \\ n_2 \end{pmatrix}, \tag{32a}$$

and by introducing the reduced composition space variables as $z_k = (n_k - n_k^*)/\mathsf{M},\ k = 1, 2$, we get

$$\begin{pmatrix} n_1 \\ n_2 \\ n_3 \\ n_4 \\ n_5 \end{pmatrix} = \begin{pmatrix} n_1^* \\ n_2^* \\ c_1 - n_2^* \\ c_2 - \frac{1}{2}n_1^* + \frac{1}{2}n_2^* \\ c_3 - \frac{1}{2}n_1^* - \frac{1}{2}n_2^* \end{pmatrix} + \mathsf{M} \begin{pmatrix} 1 & 0 \\ 0 & 1 \\ 0 & -1 \\ -\frac{1}{2} & \frac{1}{2} \\ -\frac{1}{2} & -\frac{1}{2} \end{pmatrix} \begin{pmatrix} z_1 \\ z_2 \end{pmatrix}. \tag{32b}$$

Using Eqs. (31a-31c), this system can be rewritten as

$$\mathbf{n} = \begin{pmatrix} n_1 \\ n_2 \\ n_3 \\ n_4 \\ n_5 \end{pmatrix} = \begin{pmatrix} n_1^* \\ n_2^* \\ n_3^* \\ n_4^* \\ n_5^* \end{pmatrix} + \mathsf{M} \begin{pmatrix} 1 & 0 \\ 0 & 1 \\ 0 & -1 \\ -\frac{1}{2} & \frac{1}{2} \\ -\frac{1}{2} & -\frac{1}{2} \end{pmatrix} \begin{pmatrix} z_1 \\ z_2 \end{pmatrix} = \mathbf{n}^* + \mathsf{M}\mathcal{D} \cdot \mathbf{z}. \tag{32c}$$

As we can see, this model problem is now described in the $R = 2$ dimensional reactive composition space. Using Eqs. (17a) and (18), the non-linear ODE that describes the reactive system evolution is:

$$\frac{d\mathbf{z}}{dt} = \mathbf{f}(\mathbf{z}) = \dot{\mathbf{w}}, \tag{33a}$$

where

$$\dot{\mathbf{w}} = \frac{-1}{\rho} \begin{pmatrix} r_2 - r_1 \\ r_1 + r_2 \end{pmatrix}. \tag{33b}$$

Now, for the considered system, the mixture total mass is calculated using Eq. (2a), $\mathsf{M} = 1.20 \times 10^{-1}\ g$. So, the mixture density is $\rho = 1.20 \times 10^{-4}\ g/cm^3$. Explicitly, the evolution of the system is

$$\begin{aligned} \frac{dz_1}{dt} &= 2.51 \times 10^2 + 1.16 \times 10^7 z_2 + 6.99 \times 10^8 z_2^2 - 9.98 \times 10^4 z_1 - 3.22 \times 10^9 z_2 z_1, & \text{(34a)} \\ \frac{dz_2}{dt} &= 2.51 \times 10^2 - 1.17 \times 10^7 z_2 - 6.98 \times 10^8 z_2^2 + 8.47 \times 10^4 z_1 - 1.84 \times 10^9 z_2 z_1, & \text{(34b)} \end{aligned}$$

where we note that the maximum degree of Eq. (34) is $\mathtt{d} = 2$.

1. *Finite equilibria*

The procedure described in Sec. III B is used to find the finite equilibria of the autonomous dynamical system, Eq. (33a), which describe the evolution of $\mathbf{z}$. By equilibrating the left hand side of Eq. (34) and using `Bertini` to find all the $\mathbf{z}^e$ that satisfy $\mathbf{f}(\mathbf{z}^e) = \mathbf{0}$, we find the following finite equilibria,

$$\begin{aligned} R_1 &\equiv (\mathbf{z}^e) = \left(-1.78 \times 10^{-5}, -1.67 \times 10^{-2}\right) mol/g, \\ R_2 &\equiv (\mathbf{z}^e) = \left(-4.20 \times 10^{-3}, -2.66 \times 10^{-5}\right) mol/g, \\ R_3 &\equiv (\mathbf{z}^e) = \left(3.05 \times 10^{-3}, 2.94 \times 10^{-5}\right) mol/g. \end{aligned}$$

Here, all the finite equilibria are real isolated critical points. The rest of the species are obtained from Eq. (32c):

$$\begin{aligned} R_1 &\equiv (\mathbf{n}^e) = \left(-2.14 \times 10^{-6}, -2.00 \times 10^{-3}, 4.00 \times 10^{-3}, 1.70 \times 10^{-8}, 3.00 \times 10^{-3}\right)\ mol, \\ R_2 &\equiv (\mathbf{n}^e) = \left(-5.04 \times 10^{-4}, -3.20 \times 10^{-6}, 2.00 \times 10^{-3}, 1.25 \times 10^{-3}, 2.25 \times 10^{-3}\right)\ mol, \\ R_3 &\equiv (\mathbf{n}^e) = \left(3.66 \times 10^{-4}, 3.53 \times 10^{-6}, 2.00 \times 10^{-3}, 8.19 \times 10^{-4}, 1.82 \times 10^{-3}\right)\ mol. \end{aligned}$$

It is clear that R_1 and R_2 are non-physical equilibria, while R_3 is a physical root that satisfy Eq. (23); R_3 is the reactive system's unique physical equilibrium point.

To investigate the dynamical character of each critical point, first Eq. (34) is linearized to find $\mathbf{J}^e$. Following Eq. (24) we obtain

$$\mathbf{J}^e = \begin{pmatrix} -9.98 \times 10^4 - 3.22 \times 10^9 z_2^e & 1.16 \times 10^7 + 1.40 \times 10^9 z_2^e - 3.22 \times 10^9 z_1^e \\ 8.47 \times 10^4 - 1.84 \times 10^9 z_2^e & -1.17 \times 10^7 - 1.40 \times 10^9 z_2^e - 1.84 \times 10^9 z_1^e \end{pmatrix}. \quad (35)$$

By substituting R_1, R_2, and R_3 into $\mathbf{J}^e$, linear analysis in the neighborhood of each critical point reveals that R_1 is a source, R_2 is a saddle, and R_3 is a sink. The system's eigenvalues and the corresponding eigenvectors associated with each finite critical point are:

$$R_1 \ : \ (\boldsymbol{\lambda}, \boldsymbol{\upsilon}) = (4.18 \times 10^7, 2.35 \times 10^7), ([7.00 \times 10^{-1}, 7.14 \times 10^{-1}]^T, [3.61 \times 10^{-1}, 9.33 \times 10^{-1}]^T),$$
$$R_2 \ : \ (\boldsymbol{\lambda}, \boldsymbol{\upsilon}) = (-4.64 \times 10^6, 7.11 \times 10^5), ([-9.83 \times 10^{-1}, 1.81 \times 10^{-1}]^T, [1.00, 2.89 \times 10^{-2}]^T),$$
$$R_3 \ : \ (\boldsymbol{\lambda}, \boldsymbol{\upsilon}) = (-1.73 \times 10^7, -1.91 \times 10^5), ([-1.07 \times 10^{-1}, 9.94 \times 10^{-1}]^T, [1.00, 1.79 \times 10^{-3}]^T).$$

The eigenvalues' and eigenvectors' units are $1/s$ and mol/g, respectively.

Since the finite root R_2 has only one unstable mode, *i.e.* positive eigenvalue, it is a candidate point for the 1-D SIM construction. Moreover, the system's physical fast and slow time scales are the ones associated with its physical equilibrium; R_3. These are, respectively, 5.78×10^{-8} s and 5.24×10^{-6} s, which give rise to a stiffness of $\mathcal{O}(10^2)$. So, even the two step Zel'dovich mechanism retains stiffness at $T = 4000$ K. The multi-scale nature of this system is clearly shown in Fig. 1, where the full dynamics of the evolution of the species are presented. Here, the first reaction commences at $t \sim 10^{-8}$ s, and the system enters its last relaxation toward the physical equilibrium state after $t \sim 10^{-5}$ s.

Since the system's SIM might have two branches, we now find its infinite equilibria.

2. Infinite equilibria

In addition to its three finite critical points, this system has equilibria at infinity. They can be identified using the projective space technique described in Sec. III C. Arbitrarily, we select $k = 1$, so the Zel'dovich reactive system in the projective space is realized by the

following transformation: $Z_0 = t, Z_1 = 1/z_1,\ Z_2 = z_2/z_1$. Subsequently, we have

$$\frac{dZ_0}{d\tau} = Z_1, \tag{36a}$$

$$\frac{dZ_1}{d\tau} = 9.98 \times 10^4 Z_1^2 - 2.51 \times 10^2 Z_1^3 + 3.22 \times 10^9 Z_1 Z_2 - 1.16 \times 10^7 Z_1^2 Z_2 - 6.99 \times 10^8 Z_1 Z_2^2, \tag{36b}$$

$$\frac{dZ_2}{d\tau} = 8.47 \times 10^4 Z_1 + 2.51 \times 10^2 Z_1^2 (1 - Z_2) - 1.84 \times 10^9 Z_2 - 1.16 \times 10^7 Z_1 Z_2 + 2.52 \times 10^9 Z_2^2 - 1.16 \times 10^7 Z_1 Z_2^2 - 6.99 \times 10^8 Z_2^3. \tag{36c}$$

By using `Bertini` to find all the $\mathbf{Z}^e$ that satisfy $\mathbf{F}(\mathbf{Z}^e) = \mathbf{0}$, we find three equilibria. These equilibria are

$$I_1 \equiv (\mathbf{Z}^e) = (0, 0),$$
$$I_2 \equiv (\mathbf{Z}^e) = (0, 1.01),$$
$$I_3 \equiv (\mathbf{Z}^e) = (0, 2.60),$$

and they represent the infinite equilibria of the original system, Eq. (34). Here, all the infinite equilibria are real isolated critical points.

To investigate the dynamical character of each critical point, Eqs. (36b) and (36c) are linearized to find $\mathbf{J}^e$, and the eigenvalues and corresponding eigenvectors are calculated:

$$I_1 : (\boldsymbol{\lambda}, \boldsymbol{\upsilon}) = (-1.84 \times 10^9, 0)\ ([0, 1]^T, [1.00, 4.61 \times 10^{-5}]^T),$$
$$I_2 : (\boldsymbol{\lambda}, \boldsymbol{\upsilon}) = (2.54 \times 10^9, 1.12 \times 10^9)\ ([1.00, -1.65 \times 10^{-2}]^T, [0, 1]^T),$$
$$I_3 : (\boldsymbol{\lambda}, \boldsymbol{\upsilon}) = (3.65 \times 10^9, -2.90 \times 10^9)\ ([1.00, -1.66 \times 10^{-2}]^T, [0, 1]^T),$$

where the eigenvalues' units are $g/mol/s^2$, the first eigenvector's unit is g/mol, and the second eigenvector is dimensionless.

It is clear that I_2 is a source, I_3 is a saddle with one positive eigenvalue, and I_1 is a non-hyperbolic critical point. Consequently, the Hartman-Grobman theorem is not applicable at I_1. The normal form theory[40] is utilized to investigate the dynamical character of I_1. It is found that I_1 is a saddle-node, which consists of two hyperbolic sectors, one parabolic sector, and three separatrices.[47] Only one of these separatrices is unstable. Thus, I_1 and I_3 are candidate points for constructing the system's 1-D SIM.

3. The construction of the SIM

Now, following our 1-D SIM construction procedure, the candidate points are ordered as follows: R_2, I_1, and I_3. So, starting from the unstable direction of the candidate point R_2, Eqs. (34) are numerically integrated to generate a heteroclinic orbit. This orbit approaches R_3, the reactive system's physical equilibrium point, along its slowest mode. So, the generated orbit represents the first branch of the 1-D SIM. Then, starting from the unstable direction of the candidate point I_1, Eqs. (36) are numerically integrated to generate another heteroclinic orbit. Also, this orbit approaches R_3 along its slowest mode, So, it represents the second and last branch of the reactive system's 1-D SIM, see Fig. 2. Subsequently, there is no need to check the third candidate point, I_3.

In Fig. 2, part of the system's finite phase space and the SIM are shown. It can be noted that all reaction trajectories, inside $\mathbb{S}$ and outside of it, are attracted to the 1-D SIM.

4. Relation between thermodynamics and the SIM

To examine the relationship between system's slow dynamics and thermodynamics, σ and G are calculated within $\mathbb{S}$. In a 2-D composition space, the scalar fields, G and σ, can be represented by contours. Near equilibrium these contours approach ellipses. The major axes of these ellipses are aligned with the eigenvector associated with the largest eigenvalue of that function's local Hessian matrix ($\mathbf{H}$). Similarly, the minor axes are aligned with the eigenvector associated with the smallest eigenvalue of $\mathbf{H}$. Figure 3 shows several contours of the system's Gibbs free energy and irreversibility production rate along with the constructed 1-D SIM for the Zel'dovich mechanism, Fig. 3(a) is far away from R_3, while Fig. 3(b) is an expansion in the vicinity of R_3. In Fig. 3(b) stretching has been employed to expose the difference between the contours' major/minor axes and the SIM. Even within the close neighborhood of R_3 the contours' axes are not aligned with the 1-D SIM. So, here equilibrium thermodynamics quantities cannot explain the 1-D SIM, which describes the system's preferred path toward equilibrium. Subsequently, the gradients of these thermodynamics scalar functions do not drive the system's dynamics.

In general, in the vicinity of an equilibrium point,

$$G = G|_{\mathbf{z}^e} + \left.\frac{\partial G}{\partial \mathbf{z}}\right|_{\mathbf{z}=\mathbf{z}^e} \cdot \mathbf{z} + \frac{1}{2}\mathbf{z}^T \cdot \mathbf{H}^e_G \cdot \mathbf{z} + \ldots, \tag{37a}$$

$$\sigma = \sigma|_{\mathbf{z}^e} + \left.\frac{\partial \sigma}{\partial \mathbf{z}}\right|_{\mathbf{z}=\mathbf{z}^e} \cdot \mathbf{z} + \frac{1}{2}\mathbf{z}^T \cdot \mathbf{H}^e_\sigma \cdot \mathbf{z} + \ldots, \tag{37b}$$

where $\mathbf{H}^e$ is defined as

$$H^e_{ij} = \left.\frac{\partial^2}{\partial z_i \partial z_j}\right|_{\mathbf{z}=\mathbf{z}^e}. \tag{37c}$$

Note that $\mathbf{H}^e_G$ and $\mathbf{H}^e_\sigma$ are symmetric matrices.

However, the gradients of G and σ vanish at the physical equilibrium; G and σ have global minima at $\mathbf{z}^e$. Moreover, at the equilibrium $\sigma = 0$. So, the deviations from equilibrium values are described by

$$G - G|_{\mathbf{z}=\mathbf{z}^e} = \frac{1}{2}\mathbf{z}^T \cdot \mathbf{H}^e_G \cdot \mathbf{z} + \ldots, \tag{38a}$$

$$\sigma = \frac{1}{2}\mathbf{z}^T \cdot \mathbf{H}^e_\sigma \cdot \mathbf{z} + \ldots. \tag{38b}$$

Explicitly, for the Zel'dovich model

$$\mathbf{H}^e_\sigma = \begin{pmatrix} 1.49 \times 10^{15} & -2.09 \times 10^{16} \\ -2.09 \times 10^{16} & 1.18 \times 10^{19} \end{pmatrix}, \tag{39a}$$

$$\mathbf{H}^e_G = \begin{pmatrix} 1.52 \times 10^{13} & -8.03 \times 10^{11} \\ -8.03 \times 10^{11} & 1.36 \times 10^{15} \end{pmatrix}, \tag{39b}$$

$$\mathbf{J}^e = \begin{pmatrix} -1.95 \times 10^{5} & 1.84 \times 10^{6} \\ 3.06 \times 10^{4} & -1.73 \times 10^{7} \end{pmatrix}. \tag{39c}$$

So, the eigenvalues and the eigenvectors of these matrices are given by

$$\mathbf{H}^e_\sigma : (\boldsymbol{\lambda}, \boldsymbol{\upsilon}) = (1.18 \times 10^{19}, 1.46 \times 10^{15}), ([1.78 \times 10^{-3}, -1.00]^T, [-1.00, -1.78 \times 10^{-3}]^T),$$

$$\mathbf{H}^e_G : (\boldsymbol{\lambda}, \boldsymbol{\upsilon}) = (1.36 \times 10^{15}, 1.52 \times 10^{13}), ([5.97 \times 10^{-4}, -1.00]^T, [-1.00, -5.97 \times 10^{-4}]^T),$$

$$\mathbf{J}^e : (\boldsymbol{\lambda}, \boldsymbol{\upsilon}) = (-1.73 \times 10^{7}, -1.91 \times 10^{5}), ([-1.07 \times 10^{-1}, 9.94 \times 10^{-1}]^T, [1.00, 1.79 \times 10^{-3}]^T),$$

where for each matrix the second eigenvector yields the direction of the slow mode. It is clear that these eigenvectors are not aligned with each other. For $\mathbf{J}^e$, the arc-tangent of the ratio between the second component and the first component of υ_2 defines the angle θ at

which the 1-D SIM approach R_3. Similarly, the same ratio between the second component and the first component of υ_2 of $\mathbf{H}_G^e$ and $\mathbf{H}_\sigma^e$ define the angles at which each scalar field approaches R_3. These are

$$\begin{aligned}
\theta_{SIM} &= \tan^{-1}\left(\frac{1.79\times10^{-3}}{1.00}\right) = 1.79\times10^{-3}\ rad,\\
\theta_G &= \tan^{-1}\left(\frac{-5.97\times10^{-4}}{-1.00}\right) = 5.97\times10^{-4}\ rad,\\
\theta_\sigma &= \tan^{-1}\left(\frac{-1.78\times10^{-3}}{-1.00}\right) = 1.78\times10^{-3}\ rad.
\end{aligned}$$

where all the calculations have been performed to 100 significant digits, though the listed numbers are rounded to three significant digits. Thus, even at R_3, the reactive system's SIM cannot be identified using G or σ. Indeed, at R_3 the error in σ is small; the difference between θ_{SIM} and θ_σ is $\mathcal{O}\left(10^{-5}\ rad\right)$. But, this error grows as we move away from R_3. Moreover, because they are not exactly identical, other choices of parameters would lead to larger differences.

To reinforce our point, we address this issue in more detail. Indeed, all the system's trajectories within $\mathbb{S}$ approach the equilibrium point in infinite time. This point is the global minimum of G and σ. Near equilibrium, the system's dynamics relax onto the eigenvector associated with the slowest time scale. At the equilibrium point, the eigenvector associated with the smallest eigenvalue of $\mathbf{J}^e$ defines the direction of the system's slowest mode. The major/minor axes of G and σ contours are aligned with the eigenvectors of $\mathbf{H}_G^e$ and $\mathbf{H}_\sigma^e$, respectively. However, it is easy to show that at equilibrium there is a relationship between these two Hessians.

To find this relation, we start by substituting Eq. (16a) into Eq. (13) to obtain

$$\sigma = -\frac{\mathsf{M}}{T}\sum_{i=1}^{N}\sum_{k=1}^{R}\bar{\mu}_i\mathcal{D}_{ik}\frac{dz_k}{dt}. \tag{40}$$

Also, by substituting Eq. (15) into Eq. (9a), we have

$$G = \sum_{i=1}^{N}\bar{\mu}_i\left(n_i^* + \mathsf{M}\sum_{k=1}^{R}\mathcal{D}_{ik}z_k\right). \tag{41}$$

The gradient of G with respect to the reduced composition variables $\mathbf{z}$ is given by

$$\frac{\partial G}{\partial z_k} = \mathsf{M}\sum_{i=1}^{N}\bar{\mu}_i\mathcal{D}_{ik}, \quad k = 1,\ldots,R. \tag{42}$$

Now, by substituting Eq. (17a) and Eq. (42) into Eq. (40), the irreversibility production rate is given by

$$\sigma = -\frac{1}{T}\sum_{k=1}^{R}\frac{\partial G}{\partial z_k}\dot{w}_k. \tag{43}$$

Thus, the local Hessian of σ is given by

$$\frac{\partial^2\sigma}{\partial z_i \partial z_j} = -\frac{1}{T}\sum_{k=1}^{R}\left(\frac{\partial G}{\partial z_k}\frac{\partial^2\dot{w}_k}{\partial z_i \partial z_j} + \frac{\partial^2 G}{\partial z_i \partial z_k}\frac{\partial \dot{w}_k}{\partial z_j} + \frac{\partial^2 G}{\partial z_j \partial z_k}\frac{\partial \dot{w}_k}{\partial z_i} + \frac{\partial^3 G}{\partial z_i \partial z_j \partial z_k}\dot{w}_k\right). \tag{44}$$

At equilibrium, G is minimized, and thus

$$\dot{w}_k\big|_{\mathbf{z}=\mathbf{z}^e} = 0, \quad k = 1, \ldots, R, \tag{45a}$$

$$\left.\frac{\partial G}{\partial z_k}\right|_{\mathbf{z}=\mathbf{z}^e} = 0, \quad k = 1, \ldots, R. \tag{45b}$$

Subsequently,

$$\left.\frac{\partial^2\sigma}{\partial z_i \partial z_j}\right|_{\mathbf{z}=\mathbf{z}^e} = -\frac{1}{T}\sum_{k=1}^{R}\left(\frac{\partial^2 G}{\partial z_i \partial z_k}\frac{\partial \dot{w}_k}{\partial z_j} + \frac{\partial^2 G}{\partial z_j \partial z_k}\frac{\partial \dot{w}_k}{\partial z_i}\right)_{\mathbf{z}=\mathbf{z}^e}, \tag{46a}$$

or in Gibbs notation, and using Eq. (25),

$$\mathbf{H}^e_\sigma = -\frac{1}{T}\left[(\mathbf{H}^e_G \cdot \mathbf{J}^e) + (\mathbf{H}^e_G \cdot \mathbf{J}^e)^T\right]. \tag{46b}$$

It is clear that the first term on the right hand side of Eqs. (46) is the transpose of the second term.

In the highly unusual case in which $\mathbf{H}^e_G$ is diagonal with identical eigenvalues, the SIM can be identified by consideration of the eigenvectors of $\mathbf{H}^e_\sigma$. In that case, the eigenvectors of $\mathbf{J}^e$ are aligned with those of $\mathbf{H}^e_\sigma$. However, essentially all practical reactive systems have $\mathbf{H}^e_G$ which are not diagonal and do not have identical eigenvalues. Thus, $\mathbf{H}^e_G$ operates on $\mathbf{J}^e$ in a non-uniform way, such that the eigenvalues and the eigenvectors of $\mathbf{H}^e_\sigma$ are not the same as those of $\mathbf{J}^e$. Thus, the system's dynamics cannot be deduced from σ or G. In conclusion, we can state that any approach that employes equilibrium thermodynamic potentials to deduce a reactive system's dynamics is faulty.

B. Thermodynamics-based SIM

The second example in this work is identical to the second example presented by Lebiedz.[19] A simple closed reactive system contains three species given by the following

kinetics model: $A + A \rightleftharpoons B \rightleftharpoons C$. Using the same argument, described in the original work,[19] that the total mass is conserved, the dimension of the composition space of this model problem is reduced from $N = 3$ to $N - 1 = 2$. Also, for convenience, the dimensionless variables c_A and c_B in the original work[19] are denoted here by z_1 and z_2, respectively. The evolution of the reactive system is described by[19]

$$\frac{dz_1}{dt} = 10^{-5} z_2 - z_1^2, \tag{47a}$$

$$\frac{dz_2}{dt} = z_1^2 + (1 - 1001 z_2 - z_1) \times 10^{-5}, \tag{47b}$$

which is in the form of Eq. (21), and it is clear that $\mathtt{d} = 2$.

To construct the actual SIM for this system, we use the procedure of Sec. III. For this system, two finite equilibria are found,

$$R_1 \equiv (\mathbf{z}^e) = \left(9.99 \times 10^{-5}, 9.99 \times 10^{-4}\right),$$
$$R_2 \equiv (\mathbf{z}^e) = \left(-1.00 \times 10^{-4}, 9.99 \times 10^{-4}\right).$$

The two finite equilibria are isolated points with real coordinates. Also, linear analysis in the neighborhood of each equilibrium reveals that R_1 is a sink and R_2 is a saddle. The eigenvalues and the associated eigenvectors at the equilibria are:

$$R_1 \ : \ (\boldsymbol{\lambda}, \boldsymbol{\upsilon}) = (-1.00 \times 10^{-2}, -2.00 \times 10^{-4})([-1.02 \times 10^{-3}, 1.00]^T, [1.00, 1.93 \times 10^{-2}]^T),$$
$$R_2 \ : \ (\boldsymbol{\lambda}, \boldsymbol{\upsilon}) = (-1.00 \times 10^{-2}, 2.00 \times 10^{-4})([-9.79 \times 10^{-4}, 1.00]^T, [1.00, -2.05 \times 10^{-2}]^T).$$

It is clear that R_1 is the system's unique equilibrium point, and R_2 is a candidate saddle; its eigenvalue spectrum contains only one positive eigenvalue. Since the physical equilibrium is non-trivial, a second candidate point could exist at infinity.

To investigate the existence of such equilibrium at infinity, the projective space technique is employed. By choosing $k = 2$, the projective space is realized by the following transformation: $Z_0 = t, Z_1 = z_1/z_2,\ Z_2 = 1/z_2$. The reactive system's behavior at infinity is described by the following set of ODEs,

$$\frac{dZ_0}{d\tau} = Z_2, \tag{48a}$$

$$\frac{dZ_1}{d\tau} = 10^{-5} Z_2 - Z_1^2 + 10^{-5} Z_1 Z_2 \left(1001 + Z_1 - Z_2\right) - Z_1^3, \tag{48b}$$

$$\frac{dZ_2}{d\tau} = -Z_1^2 Z_2 + 10^{-5} Z_2^2 \left(1001 + Z_1 - Z_2\right). \tag{48c}$$

For this system there are two equilibria,

$$I_1 \equiv (\mathbf{Z}^e) = (0, 0)\,,$$
$$I_2 \equiv (\mathbf{Z}^e) = (-1, 0)\,.$$

Stability analysis in the neighborhood of these equilibria reveals that I_2 is a stable proper node,[40] with $\lambda_1 = \lambda_2 = -1$, while I_1 is a non-hyperbolic critical point with $\lambda_1 = \lambda_2 = 0$. Using the normal form theory we find that I_1 is a non-hyperbolic node which consists of two hyperbolic sectors and two parabolic sectors.

Since R_2 is the only critical point with one unstable direction, it is the only candidate point for this system. Consequently, the system's SIM has only one branch. In Fig. 4, the system's SIM is presented. Several trajectories have been generated to examine the attractiveness of the SIM.

1. Global phase space

To obtain a better understanding of the dynamics of this system, sketches of the global phase portrait are illustrated in Fig. 5. Because of scaling effects, it is difficult to graphically illustrate the global dynamical behavior. First, in Fig. 5(a), the view of the projective space in the transformed coordinates is shown. Since there are two sinks for this system, R_1 and I_2, there are two basins of attraction.[49] Each basin contains only one sink, which all the trajectories inside of it approach. The shaded area represents part of the basin of attraction for R_1. Also, illustrated in dashed lines, the fast invariant manifolds of R_2 and R_1 define the boundary between the two basins and the two parts of the basin of attraction for R_1, respectively.

Next, a projection of the system's Poincaré sphere[40,50] onto a 2-D plane is presented in Fig 5(b). The Poincaré sphere is a central projection technique which maps the composition space onto a sphere, and is defined as

$$u_1 = \frac{z_1}{\sqrt{1 + z_1^2 + z_2^2}}, \tag{49a}$$
$$u_2 = \frac{z_2}{\sqrt{1 + z_1^2 + z_2^2}}, \tag{49b}$$
$$u_3 = \frac{1}{\sqrt{1 + z_1^2 + z_2^2}}. \tag{49c}$$

This technique has been used before in the literature to analyze the global dynamics of reactive systems.[17,22] The major disadvantage of this technique is that it is not a one-to-one transformation, though it is useful for analyzing low dimensional systems. In Fig. 5(b), the circle's boundary represents infinity and the shaded area is the basin of attraction for R_1. Also, $\overline{I}_1$ and $\overline{I}_2$ are antipodal points to the infinite critical points I_1 and I_2.[40] These antipodal points, or images, appear as a consequence of not using a one-to-one mapping. Figure 5 clearly shows that the constructed 1-D SIM is an accurate description of the asymptotic behavior of the system's trajectories, though it consists of only one branch.

2. SIM and MEPT

This system, described by Eq. (47), has been employed by Lebiedz[19] to present the MEPT method. The MEPT method is based on minimizing a classical thermodynamic potential, which in this case is the entropy, S. To compare the system's actual 1-D SIM to its MEPT, a series of calculations were performed to reproduce the MEPT. By following the same procedure described in the original work,[19] we were able to reconstruct the MEPT for this system. This is given by the dashed line in Fig. 6, and is identical to the one presented in Ref. 19.

Figure 6(a) is identical to Fig. 4 of Ref. 19, Fig 6(b) shows a wider range of the system's finite composition space, and Fig. 6(c) is a closer look at the system's dynamical behavior near the physical equilibrium. Figure 6 clearly shows that the MEPT is not an attractive manifold. Consequently, it cannot correspond to the SIM of the system. From Figs. 5 and 6, we can state that this particular system's SIM contains only one branch, which can be constructed by direct numerical integration starting from the candidate point R_2. In addition, no trajectory but the SIM is attractive. We note that, due to the fact that all trajectories within the basin of attraction for R_1 will approach R_1, this possibly misled the author of Ref. 19 to the incorrect conclusion that the MEPT corresponds to the SIM, or more generally that the MEPT provides an effective construction technique for systems' SIMs.

C. Simple hydrogen-oxygen reactive system

This example is adopted from Sec. II of Ren *et al.*,[21] where it serves as a model problem for illustrating how to construct the ICE-PIC manifold. Here, it is used to demonstrate the simplicity of extending our proposed technique to higher-dimensional reactive systems, and to comment on the ICE-PIC method.

The reaction mechanism contains $N = 6$ species, $L = 3$ elements, and $J = 6$ reversible reactions, see Table II. A special case in which the system is isobaric, identical to Ren *et al.*[21], will be considered. The assigned mixture temperature and pressure are $T = 3000\ K$ and $p = 1\ atm$, respectively. The initial conditions are $(n_1^* = 3.03 \times 10^{-4}, n_2^* = 1.01 \times 10^{-4}, n_3^* = 3.03 \times 10^{-4}, n_4^* = 2.32 \times 10^{-5}, n_5^* = 1.11 \times 10^{-4}, n_6^* = 3.32 \times 10^{-3})\ mol$. Here, $i = \{1, 2, 3, 4, 5, 6\}$ corresponds to the species $\{H_2, O, H_2O, H, OH, N_2\}$, respectively. This gives rise to $\mathsf{M} = 1.01 \times 10^{-1}\ g$.

The reactive system in this model problem is described in the $R = N - L = 3$ dimensional reactive composition space. The system's only constraints are the conservation of elements; thus, the ODEs that describe the system evolution are of the form

$$\frac{d\mathbf{z}}{dt} = \mathbf{f}(\mathbf{z}), \quad \mathbf{z} \in \mathbb{R}^3. \tag{50}$$

The dynamics are fully described by $\{H_2, O, H_2O\}$, and the rest of the species, $\{H, OH, N_2\}$, are given by the system's constraints, Eq. (15),

$$2n_1 + 2n_3 + 2n_4 + n_5 = 1.25 \times 10^{-3}\ mol, \tag{51a}$$

$$n_2 + n_3 + n_5 = 4.15 \times 10^{-4}\ mol, \tag{51b}$$

$$2n_6 = 6.64 \times 10^{-3}\ mol, \tag{51c}$$

which are identical to those given by Ren *et al.*[21]

The time evolution of the species is shown in Fig. 7. The multi-scale nature of this system is clearly seen. Also, it can be noted that the times at which the first reaction event commences and that at which the system relaxes onto its equilibrium are approximately $t = 10^{-9}\ s$ and $t \sim 10^{-3}\ s$, respectively.

1. The construction of the SIM

We use the method described in Sec. III to construct the SIM for this system. First, all the system's finite equilibria are identified. There are fifteen isolated critical points; eight of them are complex and seven are real. The real critical points are:

$$
\begin{aligned}
R_1 &\equiv (\mathbf{z}^e) = \left(-1.67\times10^{-1}, 3.04\times10^{-3}, 3.53\times10^{-3}\right)\ mol/g,\\
R_2 &\equiv (\mathbf{z}^e) = \left(6.44\times10^{-2}, 1.21\times10^{-2}, -7.12\times10^{-3}\right)\ mol/g,\\
R_3 &\equiv (\mathbf{z}^e) = \left(-6.47\times10^{-3}, -2.01\times10^{-2}, -2.19\times10^{-3}\right)\ mol/g,\\
R_4 &\equiv (\mathbf{z}^e) = \left(1.98\times10^{-3}, 5.04\times10^{-3}, 9.42\times10^{-3}\right)\ mol/g,\\
R_5 &\equiv (\mathbf{z}^e) = \left(-1.21\times10^{-3}, -4.45\times10^{-3}, 5.03\times10^{-3}\right)\ mol/g,\\
R_6 &\equiv (\mathbf{z}^e) = \left(2.72\times10^{-3}, 3.34\times10^{-4}, 4.72\times10^{-3}\right)\ mol/g,\\
R_7 &\equiv (\mathbf{z}^e) = \left(2.03\times10^{-3}, 3.10\times10^{-4}, 3.07\times10^{-3}\right)\ mol/g.
\end{aligned}
$$

It is clear that R_1, R_2, R_3, and R_5 are non-physical equilibria. Moreover, R_4 and R_6 are also non-physical critical points; this can be shown by computing the values of other species using the system's constraints, Eq. (51). Thus, R_7 is the system's unique physical equilibrium point, consistent with the results in Fig. 7.

Figure 8 shows part of the system's finite composition space, all the finite equilibria, and the system's $\mathbb{S}$ within the dashed simplex. The dynamical behavior analysis within the neighborhood of each critical point reveals that R_3 and R_7 are sinks, and R_1, R_2, R_4, R_5 and R_6 are saddles. The eigenvalue spectrum associated with each finite critical point is:

$$
\begin{aligned}
R_1 &: (\boldsymbol{\lambda}) = \left(-6.67\times10^{6} \pm i1.00\times10^{8}, 2.92\times10^{3}\right)\ s^{-1},\\
R_2 &: (\boldsymbol{\lambda}) = \left(1.84\times10^{14}, -1.70\times10^{14}, -1.27\times10^{12}\right)\ s^{-1},\\
R_3 &: (\boldsymbol{\lambda}) = \left(-2.97\times10^{7} \pm i2.64\times10^{7}, -1.03\times10^{5}\right)\ s^{-1},\\
R_4 &: (\boldsymbol{\lambda}) = \left(1.62\times10^{7}, 8.94\times10^{6}, -4.65\times10^{4}\right)\ s^{-1},\\
R_5 &: (\boldsymbol{\lambda}) = \left(-2.13\times10^{6} \pm i6.71\times10^{6}, 3.22\times10^{4}\right)\ s^{-1},\\
R_6 &: (\boldsymbol{\lambda}) = \left(-6.28\times10^{6} \pm i4.37\times10^{6}, 1.57\times10^{4}\right)\ s^{-1},\\
R_7 &: (\boldsymbol{\lambda}) = \left(-1.77\times10^{7}, -9.08\times10^{6}, -5.59\times10^{3}\right)\ s^{-1}.
\end{aligned}
$$

The fastest and slowest time scales associated with the physical equilibrium R_7 are $5.65\times10^{-8}\ s$ and $1.79\times10^{-4}\ s$, respectively. This will give rise to a stiffness $\mathcal{O}(10^3)$, which indicates

that the system's trajectories, inside the physical domain, will relax onto the SIM at a steep angle; the fast modes will be exhausted rapidly.

To explore the existence of equilibria at infinity, the projective space technique is employed. We select $k = 2$, though other choices would work as well. So, the reactive system in the projective space is realized by the following transformation: $Z_0 = t, Z_1 = z_1/z_2, Z_2 = 1/z_2$, and $Z_3 = z_3/z_2$. It is found for this system there are two equilibria located at infinity, but neither of them are isolated; one is a 1-D equilibrium and the other is a 2-D equilibrium. Consequently, R_1, R_2, R_5 and R_6 are the only candidate points, since the eigenvalue spectrum of the corresponding Jacobian's contains only one unstable mode.

To construct the SIM, the dynamical system, Eq. (50), is numerically integrated, starting from the candidate points, in the direction of the unstable mode pointing towards R_7. First, we generate a heteroclinic orbit starting from R_1, since it has the slowest unstable mode among the candidate points. The generated orbit connects with R_7 along its slowest mode. Thus, it represents the first branch of the system's 1-D SIM. Then, we generate another heteroclinic orbit starting from R_6. This orbit also approaches R_7 along its slowest mode to form the second branch of the 1-D SIM. Subsequently, there is no need to generate trajectories starting from the other candidate points R_2 and R_5.

The system's 1-D SIM is presented in Fig. 9. Although the SIM has been constructed and it can be illustrated, the right branch of the SIM is not presented entirely due to scaling effects. Some trajectories in Fig. 9 have been generated from inside the system's $\mathbb{S}$, while others have been initiated from its boundary. The attractiveness of the SIM is revealed by visually examining the relaxation of several trajectories rapidly onto it. This observation is consistent with our previous prediction that has been obtained based on the stiffness of the system.

2. Comparison to ICE manifold

In this section, we compare the constructed SIM with the previously published[21] ICE manifold. Calculations are first performed to reproduce the ICE manifold for the considered reactive system.

Generation of the ICE manifold is based on minimizing a classical thermodynamics potential. First, the constrained equilibrium manifold (CEM) is developed by varying one

dependent variable to minimize the system's Gibbs potential for each combination of the rest of the dependent variables. The intersection between the CEM and $\mathbb{S}$ defines a closed curve. Then, starting from several points located on the closed curve, trajectories are generated. The collection of all these trajectories provides the ICE manifold. Figure 10 shows the 1-D SIM and the 2-D ICE manifold. The computed ICE manifold is identical to that illustrated in Fig. 4 of Ren *et al.*[21]

From Fig. 10, it is clear that there are trajectories within $\mathbb{S}$ which are not attracted to the 2-D ICE manifold. However, all the system's trajectories are attracted to the 1-D SIM. Although it is difficult to visualize in Fig. 10, the 2-D ICE manifold does not contain the system's SIM: the 1-D SIM is not a subset of the 2-D ICE manifold. The error of the ICE manifold grows as we move away from R_7. Consequently, the 2-D ICE manifold cannot fully identify the system's SIM.

V. DETAILED HYDROGEN–AIR MECHANISM

In this section, the 1-D SIM for a detailed hydrogen-air kinetic system is constructed. The reactive system is based on the detailed kinetic mechanism extracted from Miller *et al.*,[51] and it has been widely used in the literature.[52–54] This mechanism consists of $J = 19$ reversible reactions involving $N = 9$ species which are composed of $L = 3$ elements, see Table III. The system is an isochoric stoichiometric hydrogen-air mixture which is initially at $p^* = 10^7\ dyne/cm^2$ and $T = 1500\ K$.

Utilizing the conservation of the three elements $\{H, O, N\}$, the $H_2 - Air$ reactive system can be described by the following autonomous dynamical system,

$$\frac{d\mathbf{z}}{dt} = \mathbf{f}(\mathbf{z}), \quad \mathbf{z} \in \mathbb{R}^6. \tag{52}$$

Here, $i = \{1, 2, 3, 4, 5, 6\}$ correspond to the species $\{H_2, O_2, H, O, OH, H_2O\}$, respectively. The rest of the species, $\{HO_2, H_2O_2, N_2\}$, are recast using Eq. (15).

The full dynamics of the species evolution are obtained by integrating Eq. (52), see Fig. 11. At $t \approx 10^{-8}\ s$, the species growth rates change slightly, which indicates that significant dissociation reactions are induced. For $10^{-7} < t < 10^{-6}\ s$, the minor species continue to increase rapidly with different growth rates. On the other hand, the major species H_2, O_2, and N_2 have essentially constant specific moles. Just past $t \approx 10^{-6}\ s$ all

the species undergo significant change, and the radicals' specific moles reach their maximum values. At $t \approx 10^{-5}\ s$, an exothermic recombination of radicals commences forming the predominant product H_2O, which continues up to $t \approx 5\ s$, after which the system approaches the equilibrium state. Figure 11 clearly illustrates the multi-scale nature of this system.

The first step in constructing the SIM, following the methodology presented in Sec. III, is to find all of the system's real isolated equilibria, finite and infinite. For this system 284 finite equilibria and 42 infinite equilibria are found. Of the finite equilibria, one is 3-D, one is 2-D, six are 1-D, and 276 are 0-D. Of the 276 0-D equilibria, 90 are real and 186 are complex. Of the 42 infinite equilibria, six are 1-D, and 36 are 0-D. Of the latter 0-D equilibria, 18 are complex and 18 are real. One of the 90 real finite critical points represents the unique physical equilibrium state of the system. This corresponds to

$$\begin{aligned} R_{19} \equiv (\mathbf{z}^e) \;=\; & \big(1.98 \times 10^{-6}, 9.00 \times 10^{-7}, 1.72 \times 10^{-9}, \\ & 2.67 \times 10^{-10}, 3.66 \times 10^{-7}, 1.44 \times 10^{-2}\big)\ mol/g. \end{aligned}$$

Then, the dynamical character of each of the 108 isolated real finite and infinite critical points is determined. It is found that among them there are only 14 candidate points for constructing the SIM; all of them are finite. The other critical points are either sources, sinks, or saddles with more than one unstable direction. By examining the trajectories that emanate from the candidate points, only two are connected with R_{19} tangent to its slowest mode via heteroclinic orbits. These two candidate points are:

$$\begin{aligned} R_{74} \equiv (\mathbf{z}^e) \;=\; & \big(6.26 \times 10^{-5}, 3.43 \times 10^{-5}, -2.30 \times 10^{-6}, \\ & 4.80 \times 10^{-7}, -1.54 \times 10^{-5}, 1.44 \times 10^{-2}\big)\ mol/g, \\ R_{79} \equiv (\mathbf{z}^e) \;=\; & \big(-3.34 \times 10^{-6}, -1.50 \times 10^{-6}, 5.27 \times 10^{-9}, \\ & 8.82 \times 10^{-10}, -6.66 \times 10^{-7}, 1.44 \times 10^{-2}\big)\ mol/g, \end{aligned}$$

and these two heteroclinic orbits combine to provide the two branches of the 1-D SIM. Figure 12 shows a 3-dimensional projection of the 1-D SIM embedded inside the 6-dimensional composition space. Since only the slow modes are present on the SIM, this 1-D manifold provides the best description of the system's slowest dynamics.

VI. CONCLUSIONS

We have presented a robust method of constructing a 1-D SIM for a closed, spatially homogenous, isothermal, reactive system described by detailed kinetics. The SIM corresponds to the exact description of the slow dynamics in the composition space of the reactive system. The construction method is based on a geometrical approach that relies upon finding and examining the dynamical behavior of all of the system's critical points. It has been shown that the construction of a 1-D SIM is algorithmically easy and computationally efficient. The resulting procedure provides a useful tool to significantly reduce the computational cost associated with modeling reactive systems. In this work, we have focused on constructing a 1-D SIM, though the method presented can be modified to construct higher-dimensional SIMs. Also, we restrict this work to isothermal reactive systems, though the method presented can be adjusted for non-isothermal reactive systems. We will report in these two aspects in the future.

We have investigated the relationship between thermodynamics and a reactive system's SIM. It has been demonstrated that a reactive system's 1-D SIM does not coincide with the path identified by minimizing a classical thermodynamic function, such as σ, S, or G, even near the equilibrium state. This point has been confirmed by a mathematical proof which shows that equilibrium thermodynamic potentials do not alone determine reactive systems' dynamics during their approach towards the physical equilibrium.

Acknowledgments

The authors recognize the support of the National Science Foundation (NSF) under grant $CBET$-0650843, and the Center for Applied Mathematics at the University of Notre Dame. A. J. Sommese and J. D. Hauenstein acknowledge the support of the Duncan Chair of the University of Notre Dame, and the NSF under grants DMS-0410047 and DMS-0712910. In addition, J. A. Diller is supported by NSF grant DMS-0653678.

[1] J. H. Seinfeld and S. N. Pandis, *Atmospheric Chemistry and Physics: From Air Pollution to Climate Change* (Wiley, New York, NY, 1998).

[2] A. L. Kuharsky and A. L. Fogelson, Biophys. J. **80**, 1050 (2001).

[3] J. F. Griffiths, Prog. Energy Combust. Sci. **21**, 25 (1995).

[4] J. M. Powers, J. Prop. Power **22**, 1217 (2006).

[5] Z. Ren and S. B. Pope, Combust. Flame **147**, 243 (2006).

[6] T. Turanyi, T. Berces, and S. Vajda, Int. J. Chem. Kinet. **21**, 83 (1989).

[7] G. Li, A. Tomlin, H. Rabitz, and J. Toth, J. Chem. Phys. **101**, 1172 (1994).

[8] L. Petzold and W. Zhu, AIChE J. **45**, 869 (1999).

[9] T. Lu and C. K. Law, Proc. Combust. Inst. **30**, 1333 (2005).

[10] U. Maas and S. B. Pope, Combust. Flame **88**, 239 (1992).

[11] V. Bykov, V. Gol'dshtein, and U. Maas, Combust. Theory Modell. **12**, 389 (2008).

[12] S. H. Lam and D. A. Goussis, Proc. Combust. Inst. **22**, 931 (1988).

[13] S. H. Lam, Combust. Sci. Technol. **89**, 375 (1993).

[14] S. H. Lam and D. A. Goussis, Int. J. Chem. Kinet. **26**, 461 (1994).

[15] M. R. Roussel and S. J. Fraser, J. Chem. Phys. **93**, 1072 (1990).

[16] M. R. Roussel and S. J. Fraser, J. Chem. Phys. **94**, 7106 (1991).

[17] M. J. Davis and R. T. Skodje, J. Chem. Phys. **111**, 859 (1999).

[18] A. N. Gorban, I. V. Karlin, and A. Y. Zinovyev, Phys. Rep. **396**, 197 (2004).

[19] D. Lebiedz, J. Chem. Phys. **120**, 6890 (2004).

[20] A. N. Gorban and I. V. Karlin, Chem. Eng. Sci. **58**, 4751 (2003).

[21] Z. Ren, S. B. Pope, A. Vladimirsky, and J. M. Guckenheimer, J. Chem. Phys. **124**, 114111 (2006).

[22] F. Creta, A. Adrover, S. Cerbelli, M. Valorani, and M. Giona, J. Phys. Chem. A **110**, 13447 (2006).

[23] F. Creta, A. Adrover, S. Cerbelli, M. Valorani, and M. Giona, J. Phys. Chem. A **110**, 13463 (2006).

[24] D. A. Goussis, M. Valorani, F. Creta, and H. N. Najm, Prog. Comp. Fluid Dyn. **5**, 316 (2005).

[25] S. Singh, J. M. Powers, and S. Paolucci, J. Chem. Phys. **117**, 1482 (2002).

[26] J. Warnatz, U. Maas, and R. W. Dibble, *Combustion* (Springer, Berlin, 1999).

[27] V. Reonhardt, M. Winckler, and D. Lebiedz, J. Phys. Chem. A **112**, 1712 (2008).

[28] J. C. Keck and D. Gillespie, Combust. Flame **17**, 237 (1971).

[29] S. Ugarte, Y. Gao, and H. Metghalchi, Int. J. Thermodynamics **8**, 43 (2005).

[30] Z. Ren, S. B. Pope, A. Vladimirsky, J. M. Guckenheimer, and M. John, Proc. Combust. Inst. **31**, 473 (2007).

[31] H. Kaper and T. Kaper, Physica D **165**, 66 (2002).

[32] M. Valorani, F. Creta, D. A. Goussis, J. C. Lee, and H. N. Najm, Combust. Flame **146**, 29 (2006).

[33] S. R. de Groot and P. Mazur, *Non-Equilibrium Thermodynamics* (Dover, New York, NY, 1984).

[34] I. Müller and W. Weiss, *Entropy and Energy: A Universal Competition* (Springer, Berlin, 2005).

[35] I. Prigogine and R. Defay, *Chemical Thermodynamics* (Longmans, London, UK, 1954).

[36] W. J. Vincenti and C. H. Kruger, *Introduction to Physical Gas Dynamics* (Wiley, New York, NY, 1965).

[37] H. B. Callen, *Thermodynamics and an Introduction to Thermostatistics* (Wiley, New York, NY, 1985).

[38] I. Prigogine, *Introduction to Thermodynamics of Irreversible Processes* (Interscience Publishers, New York, NY, 1967).

[39] J. M. Powers and S. Paolucci, Am. J. Phys. **76**, 848 (2008).

[40] L. Perko, *Differential Equations and Dynamical Systems* (Springer, New York, NY, 2001).

[41] A. J. Sommese and C. W. Wampler, *The Numerical Solution of Systems of Polynomials Arising in Engineering and Science* (World Scientific, Hackensack, NJ, 2005).

[42] D. J. Bates, J. D. Hauenstein, A. J. Sommese, and C. W. Wampler, *Bertini: Software for numerical algebraic geometry*, Available at http://www.nd.edu/∼sommese/bertini.

[43] R. J. Kee, F. M. Rupley, and J. A. Miller, *Chemkin-II: A Fortran Chemical Kinetics Package for the Analysis of Gas Phase Chemical Kinetics*, Report: SAND89-8009B (Sandia National Laboratories, Albuquerque, NM, 1992).

[44] R. J. Kee, F. M. Rupley, and J. A. Miller, *The Chemkin Thermodynamic Data Base*, Report: SAND87-8215B (Sandia National Laboratories, Albuquerque, NM, 1992).

[45] A. Morgan, *Solving Polynomial Systems Using Continuation for Engineering and Scientific Problems* (Prentice Hall, Englewood Cliffs, NJ, 1987).

[46] D. B. Shear, J. Chem. Phys. **48**, 4144 (1968).

[47] A. A. Andronov, *Qualitative Theory of Second Order Dynamical Systems* (Wiley, New York, NY, 1973).

[48] D. L. Baulch, C. T. Bowman, C. J. Cobos, R. A. Cox, T. Just, J. A. Kerr, M. J. Pilling, D. Stocker, J. Troe, W. Tsang, et al., J. Phys. Chem. Ref. Data **34**, 757 (2005).

[49] A. J. Lichtenberg and M. A. Lieberman, *Regular and Chaotic Dynamics* (Springer-Verlog, New York, NY, 1992).

[50] S. Lefschetz, *Differential Equations: Geometric Theory* (Interscience, New York, NY, 1963).

[51] J. A. Miller, R. E. Mitchell, M. D. Smooke, and R. J. Kee, Proc. Combust. Inst. **19**, 181 (1982).

[52] M. D. Smooke, J. A. Miller, and R. J. Kee, Combust. Sci. Technol. **34**, 79 (1983).

[53] F. Dabireau, B. Cuenot, O. Vermorel, and T. Poinsot, Combust. Flame **135**, 123 (2003).

[54] J. M. Powers and S. Paolucci, AIAA J. **43**, 1088 (2005).

TABLE I: Zel'dovich mechanism of nitric acid formation. The species are NO, N, O, O_2, and N_2.

j	Reaction	$A_j \ \left[cm^3/\left(mol\ s\ K^{\beta_j}\right)\right]$	β_j	$\bar{E}_j \ [cal/mol]$
1	$N + O_2 \rightleftharpoons NO + O$	5.841×10^9	1.01	6195.6
2	$N + NO \rightleftharpoons N_2 + O$	21.077×10^{12}	0.00	0.0

TABLE II: Simple hydrogen-oxygen kinetics mechanism. The species are H_2, H, O, OH, H_2O, and N_2.

j	Reaction[a]	A_j $\left[\left(mol/cm^3\right)^{\left(1-\sum_{i=1}^{N}\nu'_{ij}\right)}/s/K^{\beta_j}\right]$	β_j	$\bar{E}_j$ $[cal/mol]$
1	$O + H_2 \rightleftharpoons H + OH$	5.08×10^4	2.7	6290.0
2	$H_2 + OH \rightleftharpoons H_2O + H$	2.16×10^8	1.5	3430.0
3	$O + H_2O \rightleftharpoons 2OH$	2.97×10^6	2.0	13400.0
4	$H_2 + M \rightleftharpoons 2H + M^b$	4.58×10^{19}	-1.4	104380.0
5	$O + H + M \rightleftharpoons OH + M^b$	4.71×10^{18}	-1.0	0.0
6	$H + OH + M \rightleftharpoons H_2O + M^b$	3.80×10^{22}	-2.0	0.0

[a] Unless otherwise specified, the third body collision efficiency coefficients are unity, $\alpha = 1$.

[b] The non-unity third body collision efficiency coefficients are: $\alpha_{H_2} = 2.5, \alpha_{H_2O} = 12$.

TABLE III: Reaction mechanism rate coefficients for hydrogen-air mixture

j	Reaction[a]	$A_j \left[\left(mol/cm^3\right)^{\left(1-\sum_{i=1}^{N}\nu'_{ij}\right)}/s/K^{\beta_j}\right]$	β_j	$\bar{E}_j$ $[cal/mol]$
1	$H_2 + O_2 \rightleftharpoons 2OH$	1.70×10^{13}	0.000	47780
2	$OH + H_2 \rightleftharpoons H_2O + H$	1.17×10^{9}	1.300	3626
3	$H + O_2 \rightleftharpoons OH + O$	5.13×10^{16}	-0.816	16507
4	$O + H_2 \rightleftharpoons OH + H$	1.80×10^{10}	1.000	8826
5	$H + O_2 + M \rightleftharpoons HO_2 + M^b$	2.10×10^{18}	-1.000	0
6	$H + 2O_2 \rightleftharpoons HO_2 + O_2$	6.70×10^{19}	-1.420	0
7	$H + O_2 + N_2 \rightleftharpoons HO_2 + N_2$	6.70×10^{19}	-1.420	0
8	$OH + HO_2 \rightleftharpoons H_2O + O_2$	5.00×10^{13}	0.000	1000
9	$H + HO_2 \rightleftharpoons 2OH$	2.50×10^{14}	0.000	1900
10	$O + HO_2 \rightleftharpoons O_2 + OH$	4.80×10^{13}	0.000	1000
11	$2OH \rightleftharpoons O + H_2O$	6.00×10^{8}	1.300	0
12	$H_2 + M \rightleftharpoons 2H + M^c$	2.23×10^{12}	0.500	92600
13	$O_2 + M \rightleftharpoons 2O + M$	1.85×10^{11}	0.500	95560
14	$H + OH + M \rightleftharpoons H_2O + M^d$	7.50×10^{23}	-2.600	0
15	$H + HO_2 \rightleftharpoons H_2 + O_2$	2.50×10^{13}	0.000	700
16	$2HO_2 \rightleftharpoons H_2O_2 + O_2$	2.00×10^{12}	0.000	0
17	$H_2O_2 + M \rightleftharpoons 2OH + M$	1.30×10^{17}	0.000	45500
18	$H_2O_2 + H \rightleftharpoons HO_2 + H_2$	1.60×10^{12}	0.000	3800
19	$H_2O_2 + OH \rightleftharpoons H_2O + HO_2$	1.00×10^{13}	0.000	1800

[a] Unless otherwise specified, the third body collision efficiency coefficients are unity, $\alpha = 1$.

[b] The non-unity third body collision efficiency coefficients are: $\alpha_{H_2} = 3.3, \alpha_{H_2O} = 21$.

[c] The non-unity third body collision efficiency coefficients are: $\alpha_{H_2} = 3, \alpha_{H_2O} = 6, \alpha_H = 2$.

[d] The non-unity third body collision efficiency coefficients are: $\alpha_{H_2O} = 20$.

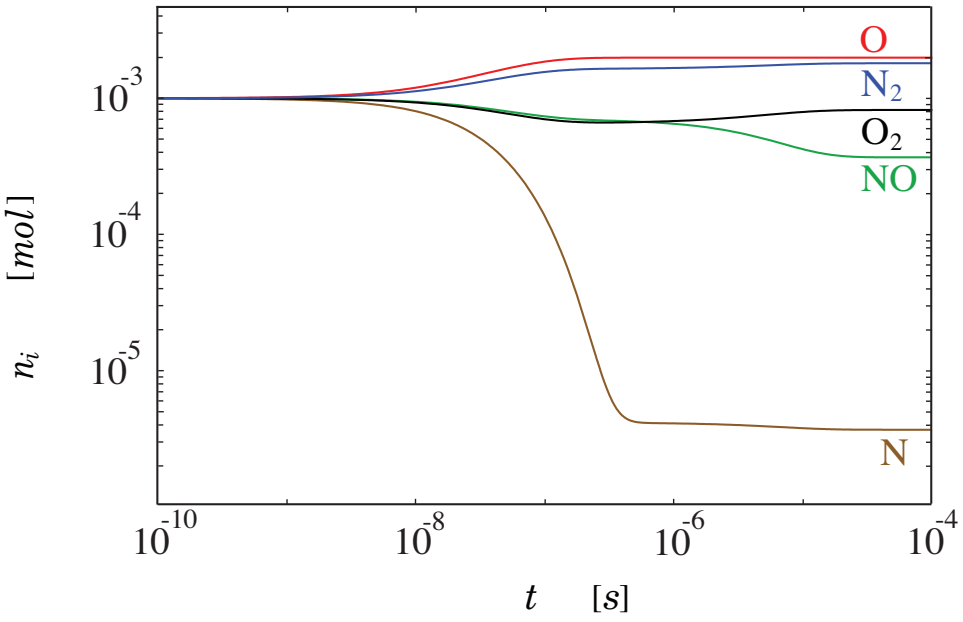

FIG. 1: The time evolution of species for the Zel'dovich model problem.

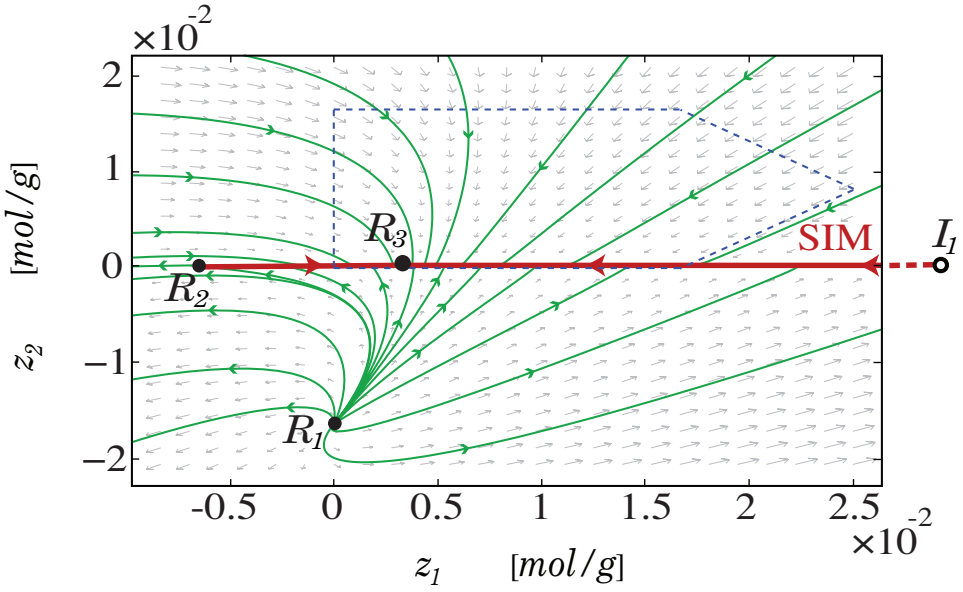

FIG. 2: A region of the finite phase space for the Zel'dovich mechanism. The solid dots represent finite critical points, the open circle represents an infinite critical point, the arrows indicate the flow directions, and the dashed simplex represents the physically accessible domain of the system; $\mathbb{S}$. The SIM is illustrated as a thick line, the thin lines represent trajectories, and R_3 represents the system's physical equilibrium state.

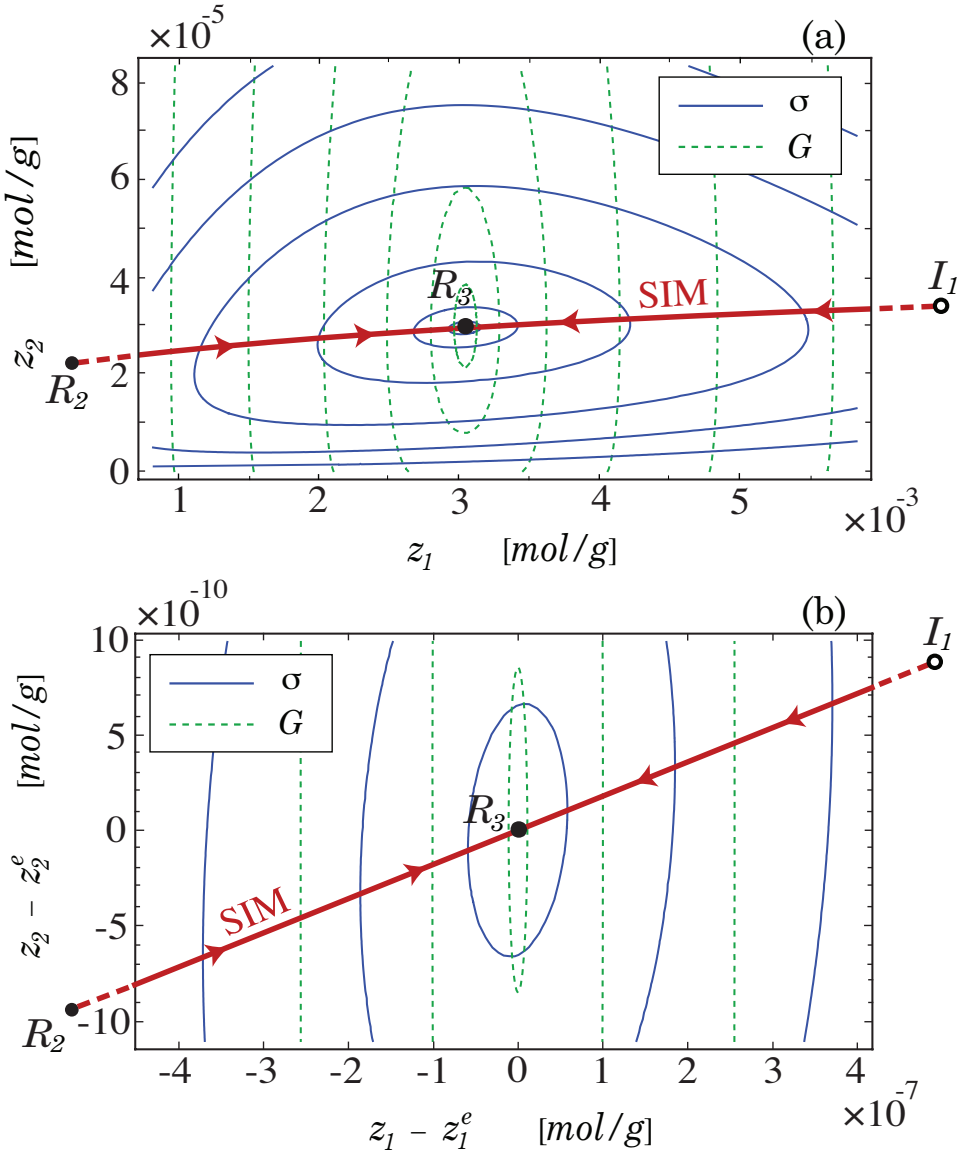

FIG. 3: (a) The SIM for the Zel'dovich mechanism near the physical equilibrium state R_3, and (b) is a blow-up of the top panel in the vicinity of R_3. The solid lines and the dashed lines represent different iso-levels of the system's irreversibility production rate and Gibbs free energy, respectively. The solid dots represent finite critical points, and the open circle represents an infinite critical point.

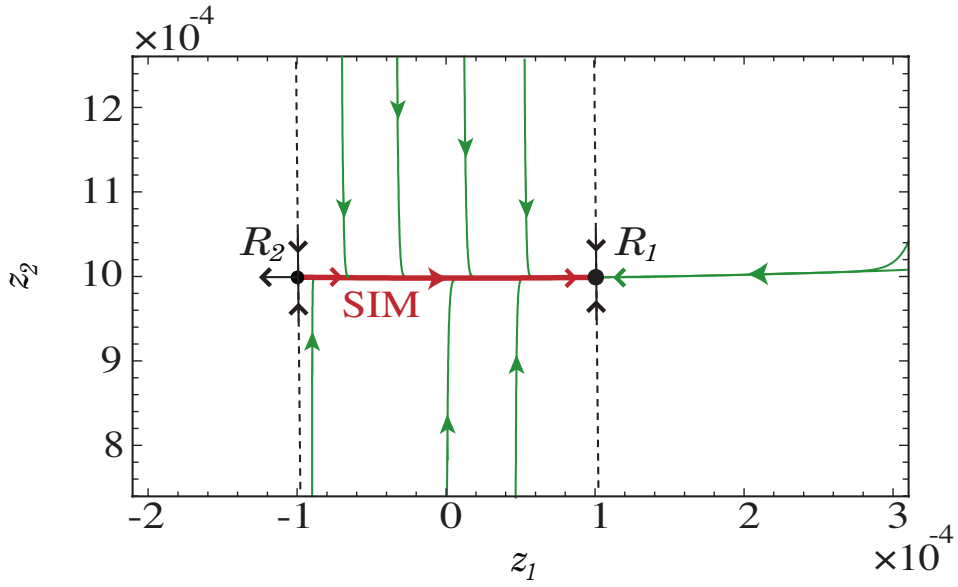

FIG. 4: A small region of the actual finite phase space for Lebiedz system.[19] The thick line is the SIM, the thin lines represent trajectories, the dashed lines represent the fast invariant manifolds, and the arrows indicate the flow directions. R_2 is a non-physical finite critical point and R_1 represents the system's physical equilibrium point.

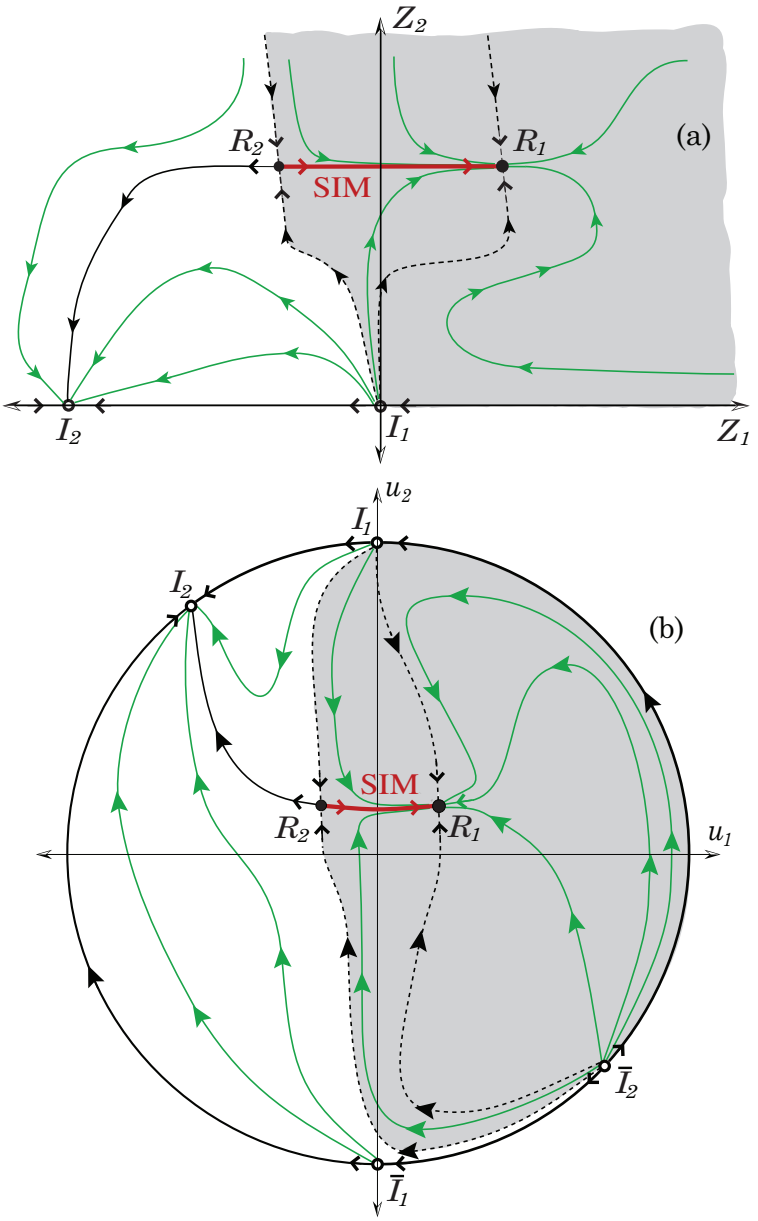

FIG. 5: Sketches of (a) the projective space portrait and (b) the global phase portrait for Lebiedz system.[19] Solid dots represent finite critical points, the shaded area represents the basin of attraction of the system's physical equilibrium state R_1, the thick line represents the SIM, the dashed lines represent the fast invariant manifolds, and the thin lines are trajectories. Open circles denote critical points at infinity and their images ($\bar{I}_i$).

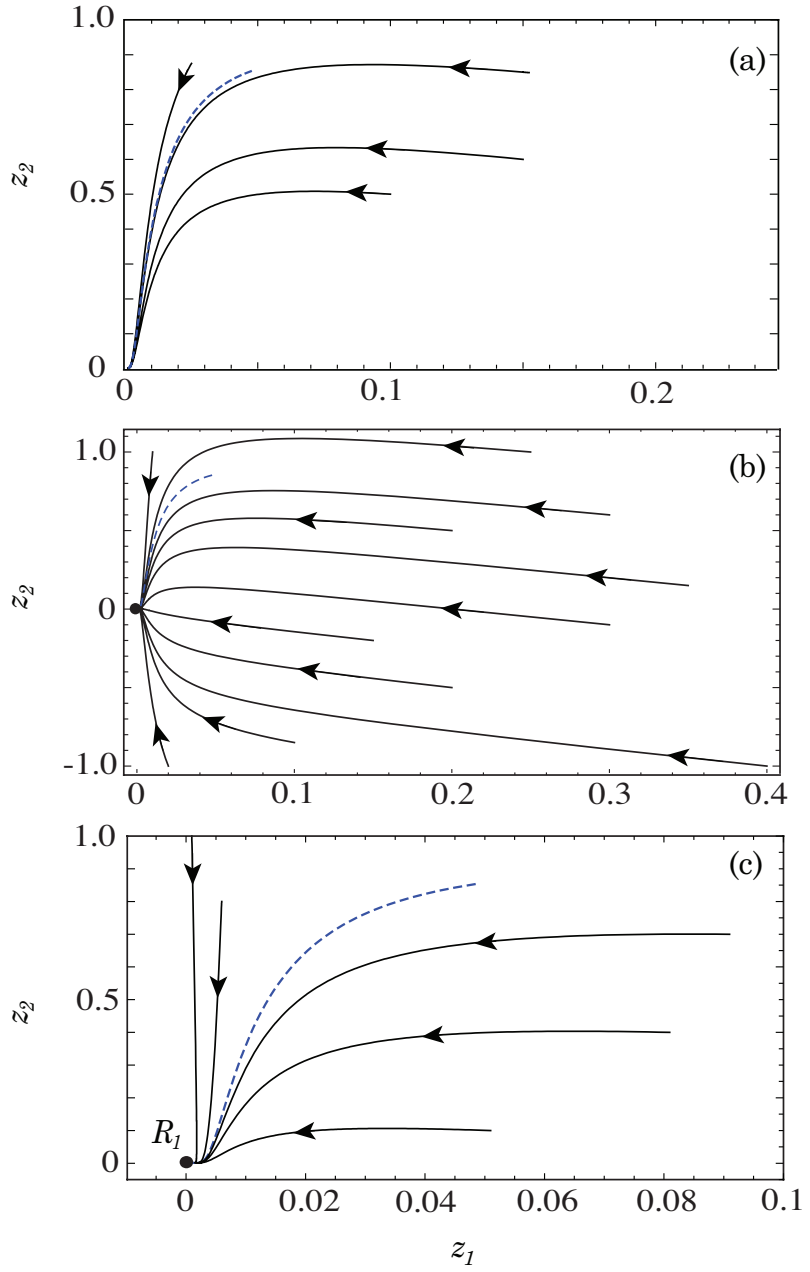

FIG. 6: The dashed line represents the calculated MEPT and the thin lines represent trajectories in the phase space of the Lebiedz system.[19] Figure (a) is identical to Fig. (4) in Ref. 19, while (b) is a wider range of the system's finite composition space, and (c) is a blow-up near the system's physical equilibrium, R_1. Different set of trajectories are illustrated in each figure.

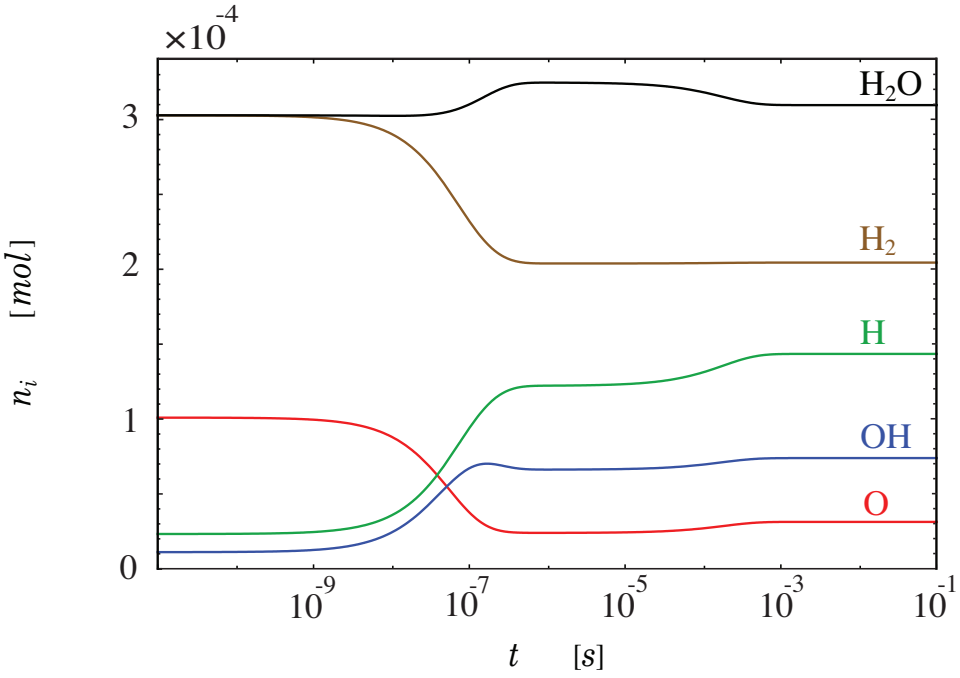

FIG. 7: The time evolution of species for the simple hydrogen-oxygen reactive system, identical to that Ren *et al.*[21]

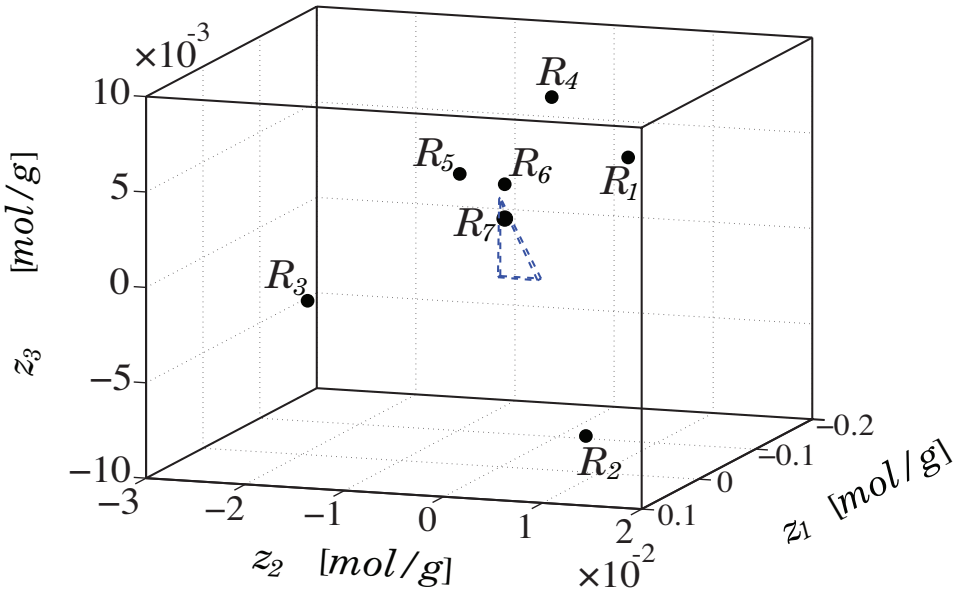

FIG. 8: A region of the finite phase space for the simple hydrogen-oxygen reactive system.[21] The dashed simplex represents the physically accessible domain of the system $\mathbb{S}$, the solid dots represent finite equilibria, and the unique critical point inside the polygon, R_7, represents the physical equilibrium point.

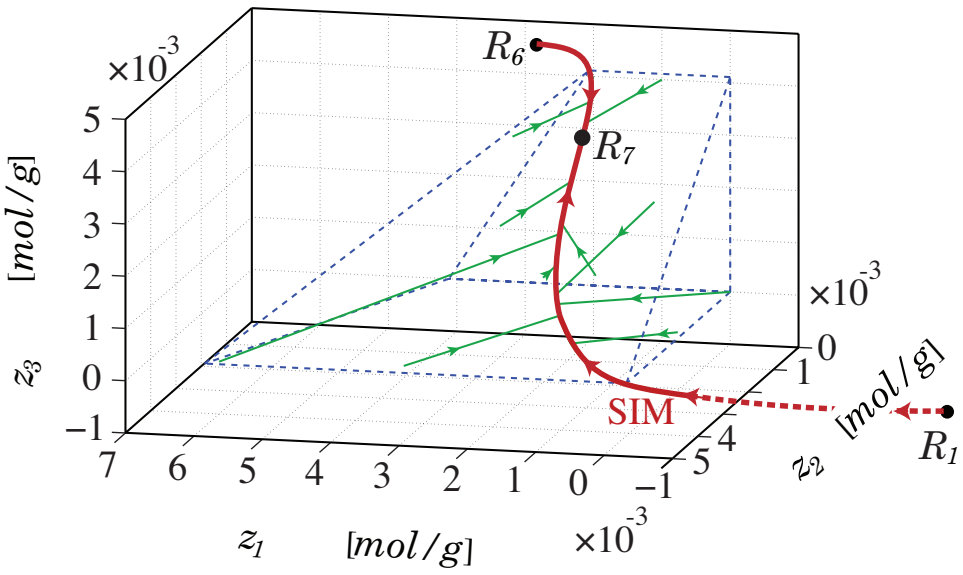

FIG. 9: The SIM for the simple hydrogen-oxygen reactive system as a thick line. The solid dots represent finite critical points, R_7 represents the system's physical equilibrium state, the dashed simplex represents $\mathbb{S}$, and the thin lines illustrate several trajectories.

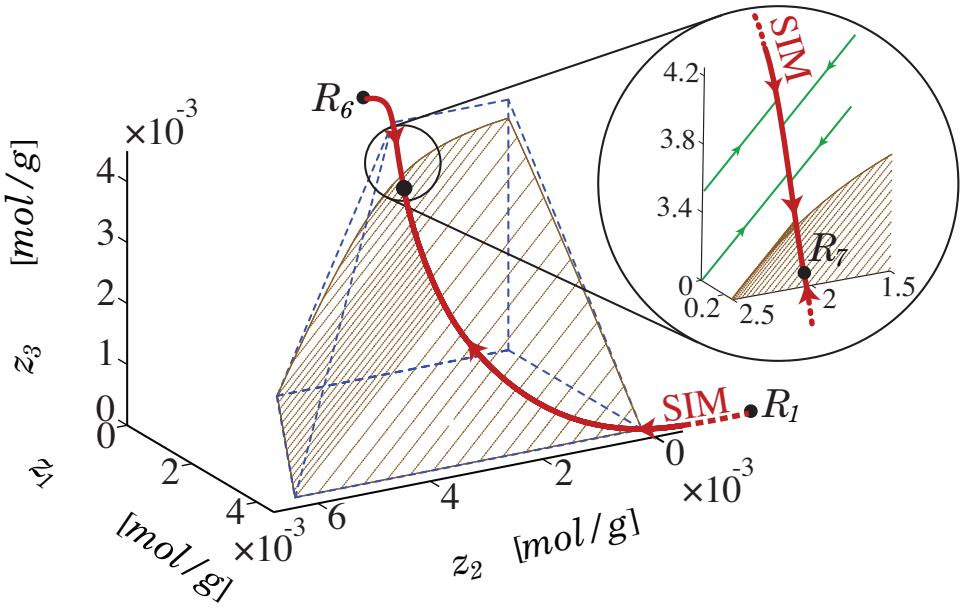

FIG. 10: A comparison between the actual 1-D SIM, illustrated as thick line, and the 2-D ICE manifold for the simple hydrogen-oxygen reactive system. The solid dots represent finite critical points, R_7 represents the system's physical equilibrium state, and the dashed simplex represents $\mathbb{S}$. Thin lines represent trajectories inside $\mathbb{S}$. The ICE manifold is identical to the one presented in Ref. 21.

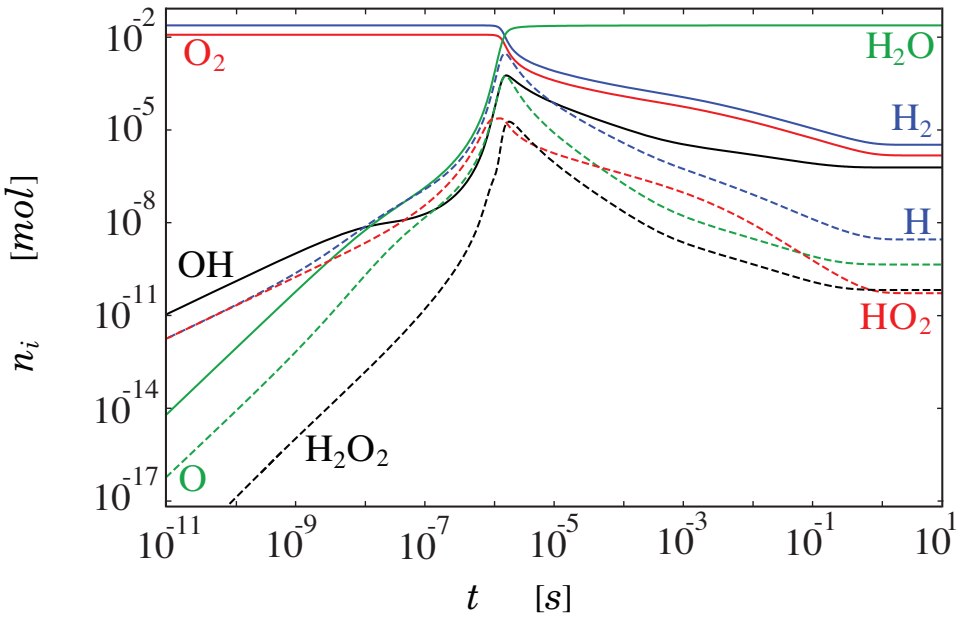

FIG. 11: The time evolution of species for the hydrogen-air reactive system.

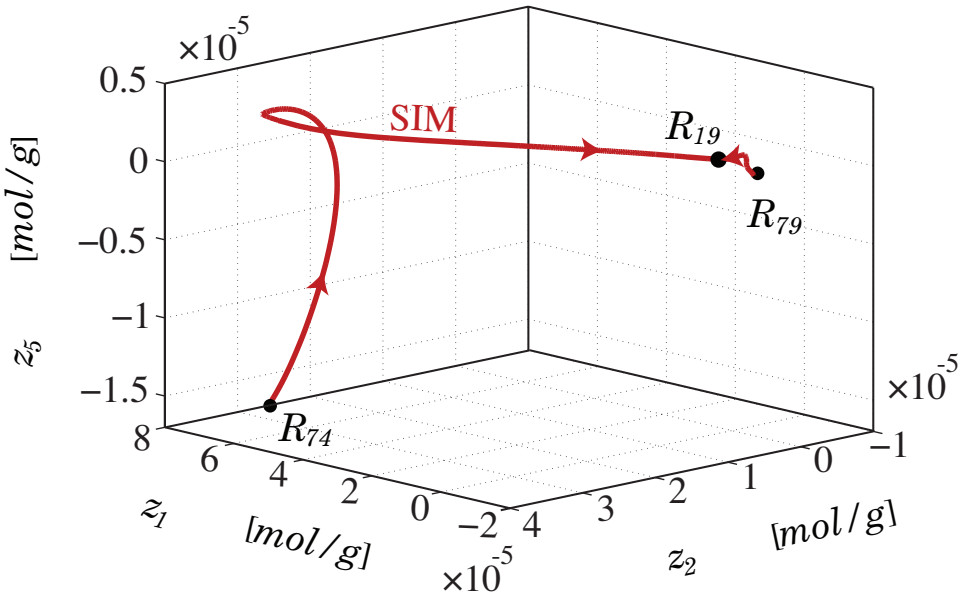

FIG. 12: The 1-D SIM for the detailed $H_2 - Air$ mechanism. The solid dots represent finite critical points, and R_{19} represents the system's physical equilibrium state.